Dynamic correlations in the conserved Manna sandpile

Anirban Mukherjee and Punyabrata Pradhan
Department of Physics of Complex Systems, S. N. Bose National Centre for Basic Sciences, Block-JD, Sector-III, Salt Lake, Kolkata 700106, India

(Received 25 November 2022; accepted 20 January 2023; published 9 February 2023)

We study dynamic correlations for current and mass, as well as the associated power spectra, in the one-dimensional conserved Manna sandpile. We show that, in the thermodynamic limit, the variance of cumulative bond current up to time T grows subdiffusively as $T^{1/2-\mu}$ with the exponent $\mu \geqslant 0$ depending on the density regimes considered and, likewise, the power spectra of current and mass at low frequency f varies as $f^{1/2+\mu}$ and $f^{-3/2+\mu}$, respectively. Our theory predicts that, far from criticality, $\mu = 0$ and, near criticality, $\mu = (\beta+1)/2\nu_\perp z > 0$ with β, $\nu_\perp$, and z being the order parameter, correlation length, and dynamic exponents, respectively. The anomalous suppression of fluctuations near criticality signifies a "dynamic hyperuniformity," characterized by a set of fluctuation relations, in which current, mass, and tagged-particle displacement fluctuations are shown to have a precise quantitative relationship with the density-dependent activity (or its derivative). In particular, the relation, $\mathcal{D}_s(\bar{\rho}) = a(\bar{\rho})/\bar{\rho}$, between the self-diffusion coefficient $\mathcal{D}_s(\bar{\rho})$, activity $a(\bar{\rho})$ and density $\bar{\rho}$ explains a previous simulation observation [Eur. Phys. J. B **72**, 441 (2009)] that, near criticality, the self-diffusion coefficient in the Manna sandpile has the same scaling behavior as the activity.

DOI: 10.1103/PhysRevE.107.024109

I. INTRODUCTION

Long-ranged temporal correlations are ubiquitous in nature [1]. They usually manifest as the so-called "$1/f$" or the flicker noise, having a characteristic low-frequency power spectra with a power-law form $1/f^{\psi}$, where $0 < \psi < 2$, over a wide range of frequency f. In fact, the $1/f$ noise has been seen in a variety of seemingly unrelated systems, such as solar flares [2,3], forest fires [4], electrical activities in brain [5,6], stock-market fluctuations [7], water flow in rivers [1] and resistance fluctuations in conductors [8], among others; for details, see reviews [9,10]. However there is no general theory explaining the relative abundance of $1/f$ noise in nature.

Bak, Tang, and Wiesenfeld (BTW) proposed sandpiles as paradigmatic models of "self-organized criticality" (SOC) in order to provide a generic mechanism for long-ranged correlations in natural systems, and $1/f$ noise in particular [11,12]. Sandpiles are spatially extended and threshold-activated systems, in which dynamical activities spread through cascades of toppling events (initialed when a local threshold is crossed), resulting in "avalanche-like" dynamical activities and long-ranged correlations in the systems. They were envisaged as model systems driven by slow addition of "energy," or grains, with local energy conservation in the bulk and dissipation at the boundary. Due to an intriguing interplay between drive and dissipation, the system evolves, apparently without fine-tuning of any parameters, towards a nonequilibrium steady state characterized through avalanches at all scales, i.e., a scale-invariant critical state with power-law distributions concerning various observables. Later, several variants, known as the conserved or "*fixed-energy*" sandpiles, were proposed, where there is no dissipation, but the total number of grains (or total energy) remains conserved, thus allowing the critical state to be reached by tuning the global density.

There have been numerous studies of sandpiles, and significant progress has been made in characterizing the static and dynamic properties of both critical and off-critical states of the systems. However, apart from some exact [13–16] and mathematically rigorous [17–19] results, the majority of the studies have been carried out using simulations [20–22] and phenomenological field-theoretical descriptions [23–25]. This is primarily due to the fact that the steady-state measure of a driven interacting-particle system such as sandpiles is in most cases *a priori* unknown and, as a result, analytic calculations, beginning with a microscopic dynamical description, prove to be quite challenging [24,26,27]. Perhaps not surprisingly, despite the fact that an explanation of $1/f$ noise was the main motivation for BTW's introduction of sandpile models, a good theoretical understanding of their time-dependent properties, particularly the exact hydrodynamics and the related transport coefficients governing the large-scale relaxations, remains lacking [28–32]. Another fascinating aspect of sandpiles has only recently been discovered. That is, the critical state of sandpiles can be *hyperuniform* [33,34], meaning that the static subsystem mass fluctuations scale with subsystem size in an anomalously slow manner [35,36]. However, we currently have a limited knowledge of hyperuniform states of matter, and one can only speculate as to how such a state emerges dynamically in the first place [37]. In fact, except for a few exact results concerning static properties of the hyperuniform state [38,39], there has been little theoretical progress in this direction and a systematic approach for identifying the precise microscopic dynamical origin of the anomalous fluctuations remains elusive. In this scenario, a closer examination of the

underlying dynamical mechanism that results in such a state is desirable.

Here we address the above issues in the context of conserved stochastic sandpiles and specifically focus on a continuous-time variant of the celebrated Manna sandpile [21,40], which has drawn a lot of attention in the past [29]. The conserved Manna sandpile is a paradigm for systems exhibiting a nonequilibrium *absorbing phase transition* from a dynamically active state to an absorbing state having no activities upon tuning the global density. In fact, through several simulation studies in the recent past, it is known that the critical state of the conserved Manna sandpile is indeed hyperuniform [33]. In other recent studies, it has been shown that the (near-)critical state is characterized by the singular transport coefficients, leading to anomalous relaxation and particle transport in the system [41,42].

Historically, time-dependent properties of sandpiles have been studied in terms of power spectra of dynamical activity such as instantaneous toppling events in the systems [43,44]. In the original slowly driven version of sandpiles, BTW reported $1/f^{\psi}$ power-law behavior of the power spectrum for the activity, with the exponent $\psi < 2$ [11], although their claim was refuted when several simulation studies later found the exponent $\psi = 2$ [43,45]. Subsequently, however, a more careful scaling analysis of simulation data revealed a nontrivial power spectra with the exponent $\psi < 2$ [44]. On the theoretical front, a dynamic renormalization-group analysis of phenomenological field-theoretical equations describing a "running" sandpile (driven with nonzero rate of grain addition) allowed an analytical calculation of the exponents ψ, involving activity as well as output current, where $1/f$-type noise was observed, with $\psi = -1$; quite interestingly, the temporal correlations in the long-time regime were found to be *anticorrelated*, with $\psi = -1 < 0$. This could well be the earliest signature of "*dynamic hyperuniformity*" in sandpiles. Recently, this particular aspect of dynamic hyperuniformity, i.e., hyperuniformity in the temporal domain, was also analyzed in a variant of the slowly driven sandpiles, called the Oslo rice pile [46]. Similar low-frequency behavior of the activity power spectrum with $\psi = -1$ (i.e., anticorrelated) was observed in Ref. [47] for a directed deterministic sandpile on a ladder with a finite driving rate; in the slow-driving limit though, Maslov *et al.* [48] previously showed that the model exhibits a $1/f^{\psi}$ power spectrum, with $\psi = 1$, for the total mass fluctuation. In a slightly different study [49] of a driven sandpile, albeit on a periodic domain, the power-spectrum of activity had been found to be $1/f^{\psi}$ with $\psi = 1$. In a conserved deterministic lattice gas in two dimensions [50], subsystem mass fluctuation was found to exhibit the power spectrum $S_M(f) \sim f^{-\psi_M}$, where $\psi = 1.5$ away from criticality and $\psi \approx 1.8$ near criticality.

In this paper, we theoretically investigate the time-dependent correlations for current and mass in the (quasi-)steady state of the one-dimensional conserved Manna sandpile. We begin with a microscopic dynamical description of the model and then introduce a new, albeit approximate, closure scheme that allows us to analytically calculate the time-dependent correlation functions for current and mass, as well as the corresponding power spectra. We establish a direct quantitative relationship between various static and dynamic fluctuation properties in terms of the density-dependent activity—the system's "order parameter," and its derivative. The main results of our paper are summarized as following.

(1) *Time-integrated bond current fluctuation.* We show that, in the thermodynamic limit, with system size $L \to \infty$ and density $\bar{\rho}$ fixed, the variance of the local (bond) current $\mathcal{Q}(T)$ up to time T grows subdiffusively with time. That is, we have $\langle \mathcal{Q}^2(T) \rangle \sim T^{\alpha}$, where, away from criticality (in the time regime $T \ll L^2$), the exponent $\alpha = 1/2$ and, near criticality (in the regime $T \ll L^z$), the current fluctuation is further suppressed with the exponent $\alpha = 1/2 - \mu$, where $\mu = (\beta + 1)/2\nu_{\perp} z > 0$ and β, $\nu_{\perp}$, and z are the activity, correlation length, and dynamic exponents, respectively; thus the anomalous suppression of the current fluctuation near criticality serves as the *dynamic precursor* to the hyperuniform state formed at the critical point.

(2) *Power spectrum of current.* We find that the time-dependent (two-point) correlation function for the instantaneous current is long-ranged (power-law) and negative, resulting in the low-frequency behavior of the corresponding power spectrum $S_{\mathcal{J}}(f) \sim f^{\psi_{\mathcal{J}}}$, which vanishes at low frequency where $\psi_{\mathcal{J}} = 1/2$ away from criticality (strictly speaking, in the time regime $1/L^2 \ll f \ll 1$ for finite L) and $\psi_{\mathcal{J}} = 1/2 + \mu$ near criticality (in the time regime $1/L^z \ll f \ll 1$).

(3) *Power spectrum of mass.* We show that the power spectrum $S_M(f)$ for subsystem-mass fluctuation on the other hand diverges $S_M(f) \sim f^{-\psi_M}$ at low frequency, where $\psi_M = 3/2$ away from criticality ($1/L^2 \ll f \ll 1$) and $\psi_M = 3/2 - \mu$ near criticality ($1/L^z \ll f \ll 1$). These two exponents are not independent though and they are connected by a scaling relation $\psi_M = 2 - \psi_{\mathcal{J}}$.

(4) *Time-integrated subsystem current fluctuation.* In the opposite limit of $T \to \infty$ (more specifically, $T \gg L^2$), with system size L finite (but, still large) and density $\bar{\rho}$ fixed, the scaled current fluctuation in the steady state is shown to be proportional to the activity $a(\bar{\rho})$ as $\lim_{T\to\infty} \langle \mathcal{Q}^2(T) \rangle / T = 2a(\bar{\rho})/L$. On the other hand, the steady-state fluctuation of the subsystem current $\bar{Q}(l, T)$, i.e., the cumulative (summed over bonds) current in a subsystem of size l, in the thermodynamic limit ($L \to \infty$) interestingly depends on the order of the limits taken. When the infinite-subsystem-size limit is taken first and then the infinite-time limit, the scaled subsystem current fluctuation $\sigma^2_{\bar{Q}}(\bar{\rho}) \equiv \lim_{l\to\infty} \lim_{T\to\infty} \langle \bar{Q}^2(l, T) \rangle / lT = 2a(\bar{\rho})$ converges to twice the activity.

(5) *Subsystem mass fluctuation and a fluctuation relation.* We derive a nonequilibrium fluctuation relation, $\sigma^2(\bar{\rho}) = \sigma^2_{\bar{Q}}(\bar{\rho})/2D(\bar{\rho})$, which connects the (scaled) subsystem mass fluctuation $\sigma^2(\bar{\rho}) = \langle M_l^2 \rangle - \langle M_l \rangle^2$, with M_l being mass in a subsystem of size l and $D(\bar{\rho})$ the density-dependent bulk-diffusion coefficient, to the (scaled) subsystem current fluctuation. Remarkably, the relation explains why the mass fluctuation in the Manna sandpile must vanish upon approaching criticality and thus helps characterize the dynamical origin of hyperuniformity in the system.

(6) *Self-diffusion coefficient of tagged particles.* We also study the steady-state mean-square displacements of tagged particles, which are characterized by the self-diffusion coefficient of the individual particle. We theoretically show that

the self-diffusion coefficient $\mathcal{D}_s(\bar{\rho})$ is identically equal to the ratio $a(\bar{\rho})/\bar{\rho}$ of the activity to the global number density of the system, i.e., $\mathcal{D}_s(\bar{\rho}) = a(\bar{\rho})/\bar{\rho}$, a fluctuation relation, which connects the (scaled) tagged-particle displacement fluctuation to the density-dependent activity. This relation immediately explains a previous simulation observation of Ref. [27] that, upon approaching criticality, the self-diffusion coefficient in the conserved Manna sandpile vanishes in the same fashion as the activity. Our theoretical results are in a reasonably good agreement with simulations.

The plan of the paper is as follows: In Sec. II A, we define the conserved Manna sandpile and the various quantities of interest. In Sec. II B, we present our calculation method where we introduce an approximate truncation scheme, helping us to calculate the dynamic correlations. Then in Sec. II C, we study the dynamic properties of bond current fluctuations in the system and provide a scaling argument to explain its behavior near criticality, followed by the calculation of the corresponding power spectrum in Sec. II D 1. We then proceed to calculate the variance of the cumulative subsystem (i.e., space-time integrated) current and elucidate its relationship with the particle mobility in Sec. II D 3. We study the self-diffusion coefficient of tagged particles and the power spectrum for subsystem mass fluctuation in Secs. II E and II F, respectively. Finally, in Sec. III, we summarize with some concluding remarks.

II. DYNAMIC CORRELATIONS IN THE STEADY STATE

A. Model and definitions

We consider the continuous-time variant [21] of the conserved ("fixed energy") Manna sandpile [40] on a ring of L sites. Any site i, with $i = 0, 1, \ldots, L-1$, can have $m_i \geqslant 0$ number of particles, with $m_i = 0, 1, \ldots, N$; the total number of particles

$$N = \sum_{i=0}^{L-1} m_i \tag{1}$$

remains *conserved*; in this paper we throughout denote the global density as $\bar{\rho} = N/L$. The dynamical rules are as follows: An *active* site—a site with $m_i > 1$—topples with rate 1 by randomly and independently transferring each of the two particles to one of its nearest neighbors.

The sytem violates detailed balance and eventually reaches a nonequilibrium (quasi-)steady state, which is not described by the familiar equilibrium Boltzmann-Gibbs distribution and whose probability measure is *a priori* unknown. The steady state of the system is usually characterized through a global order parameter, called the activity $a(\bar{\rho})$, defined as the density of active sites,

$$a(\bar{\rho}) = \frac{\langle N_a \rangle}{L}, \tag{2}$$

where N_a is the total number of active sites in the system and $\langle . \rangle$ denotes the steady-state average. Interestingly the system has a nontrivial spatiotemporal structure and, upon tuning the global density $\bar{\rho}$, undergoes an absorbing phase transition. That is, above a critical density ρ_c, there are dynamical activities in the system, but, below the critical density, the dynamical activities in the steady state cease and consequently there are no movements of particles in the system. The absorbing phase transition in the conserved Manna sandpile has been intensively studied in the past and can be characterized by the following critical exponents—the order-parameter exponent β, the correlation-length exponent $\nu_\perp$, and the dynamic exponent z: Upon approaching criticality from above, we have the following scaling behavior of activity $a(\Delta) \sim \Delta^\beta$, correlation length $\xi \sim \Delta^{-\nu_\perp}$, and the relaxation time $\tau_r \sim L^z$ where relative density $\Delta = \bar{\rho} - \rho_c > 0$ and we use the critical density $\rho_c \approx 0.948\,85$, as estimated in Ref. [21], throughout our paper.

One can write update rules in an infinitesimal time-interval between time t and $t + dt$ as given below,

$$m_i(t+dt) = \begin{cases} \textit{events} & \textit{probabilities} \\ m_i(t)+1 & \frac{1}{2}\hat{a}_{i+1}dt \\ m_i(t)+1 & \frac{1}{2}\hat{a}_{i-1}dt \\ m_i(t)+2 & \frac{1}{4}\hat{a}_{i+1}dt \\ m_i(t)+2 & \frac{1}{4}\hat{a}_{i-1}dt \\ m_i(t)-2 & \hat{a}_i dt \\ m_i(t) & [1-\Sigma dt], \end{cases} \tag{3}$$

where $\Sigma = (3/4)(\hat{a}_{i+1} + \hat{a}_{i-1}) + \hat{a}_i$; here $\hat{a}_i$ is an indicator function with $\hat{a}_i = 1$ if the site is active and $\hat{a}_i = 0$ otherwise. Using the above update rules (3), we can write the time evolution equation of the first moment of local mass as

$$\frac{d}{dt}\langle m_i(t)\rangle = [\langle \hat{a}_{i-1}(t) - 2\hat{a}_i(t) + \hat{a}_{i+1}(t)\rangle]. \tag{4}$$

Denoting the local density $\rho_i(t) = \langle m_i(t)\rangle$, we can alternatively write the above equation as

$$\frac{d}{dt}\rho_i(t) = \sum_k \Delta_{i,k} a_k(t), \tag{5}$$

where $\Delta_{i,k}$ is the discrete Laplacian and $a_k(t) = \langle \hat{a}_k \rangle(t)$ is the average instantaneous activity. On the large spatiotemporal scales and by taking the diffusive scaling limit $i \to x = i/L$ and $t \to \tau = t/L^2$, we can write the hydrodynamic time-evolution equation for the local density field $\rho(x,\tau)$ as in Eq. (5) [41,42],

$$\frac{\partial \rho(x,\tau)}{\partial \tau} = \frac{\partial^2 a(\rho)}{\partial x^2} \equiv \frac{\partial}{\partial x}\left(D(\rho)\frac{\partial \rho}{\partial x}\right), \tag{6}$$

where $D(\rho)$ is the density-dependent bulk-diffusion coefficient. It has been previously demonstrated in Refs. [41,42], the bulk-diffusion coefficient can be written in terms of the derivative of the activity $a(\rho)$ with respect to density ρ,

$$D(\rho) = \frac{da(\rho)}{d\rho} \equiv a'(\rho). \tag{7}$$

Indeed the relaxation processes occurring on a large (coarse-grained) scale are primarily governed by the bulk-diffusion coefficient—the fact that we later use to introduce a truncation scheme [see Eq. (23)] for analytically calculating various time-dependent correlation functions, which would not have been possible otherwise in a system with nontrivial correlations as in sandpiles. Notably, one can recast the density evolution equation (5) in a microscopic form of the continuity

equation,

$$\frac{d}{dt}\rho_i(t) = \langle \mathcal{J}_i(t) - \mathcal{J}_{i+1}(t)\rangle, \tag{8}$$

where the microscopic instantaneous current $\mathcal{J}_i(t)$ is defined as the number of particles crossing a bond $(i, i+1)$ in an infinitesimal time interval $(t, t+dt)$. It is useful to define a related observable—the cumulative, or time-integrated, bond current $\mathcal{Q}_i(t)$ up to time t, which is used to calculate various other correlation functions, such as that involving mass and activity, and is easily measured in simulations. At the microscopic level, the time-integrated current $\mathcal{Q}_i(t)$ is defined as the total number of particles transferred across the ith bond, connecting the nearest-neighbor pair of sites $(i, i+1)$ during a time interval $[0, t]$. That is, the time-integrated current across the ith bond during an infinitesimal time interval $[t, t+dt]$ is simply $\mathcal{J}_i(t)dt$ with

$$\mathcal{J}_i(t) = \lim_{\Delta t\to 0}\frac{\mathcal{Q}_i(t+\Delta t) - \mathcal{Q}_i(t)}{\Delta t} \equiv \frac{d\mathcal{Q}_i(t)}{dt}, \tag{9}$$

and

$$\mathcal{Q}_i(T) = \int_0^T dt\,\mathcal{J}_i(t). \tag{10}$$

On the average level, we therefore have

$$\langle \mathcal{J}_i(t)\rangle = \left\langle \frac{d\mathcal{Q}_i(t)}{dt}\right\rangle = \frac{d\langle \mathcal{Q}_i(t)\rangle}{dt}. \tag{11}$$

We now decompose the instantaneous current into two parts—a diffusive component $\mathcal{J}_i^{(d)}(t)$ and a fluctuating component $\mathcal{J}_i^{(fl)}(t)$,

$$\mathcal{J}_i(t) = \mathcal{J}_i^{(d)}(t) + \mathcal{J}_i^{(fl)}(t), \tag{12}$$

where, motivated by Eq. (4), we identify the diffusive current as

$$\mathcal{J}_i^{(d)}(t) = \hat{a}_i(t) - \hat{a}_{i+1}(t). \tag{13}$$

Indeed, as we see later, in that case only the diffusive-current component possesses long-ranged temporal correlations, varying slowly in time as a power law, and the fluctuating component on the other hand is simply a delta-correlated one, explaining the motivation behind the above decomposition. Note that, due to the fact $\langle \mathcal{J}_i\rangle = \langle \mathcal{J}_i^{(d)}\rangle = \langle \hat{a}_i\rangle - \langle \hat{a}_{i+1}\rangle$, we must have $\langle \mathcal{J}_i^{(fl)}\rangle = 0$. Indeed the fluctuating current component can be related to the (conserved) noise term in an appropriately coarse-grained fluctuating hydrodynamic theory, which can be then used to study the large-scale fluctuation properties of the system [51,52].

In the following sections, we study the fluctuation properties of various components of currents, instantaneous and the fluctuating one as decomposed in Eq. (13). Throughout the paper, we use the following notation for correlation function $C_r^{AB}(t, t')$ involving any two local observables $A_i(t)$ and $B_j(t')$ with $t \geqslant t'$:

$$C^{AB}_{r=|i-j|}(t, t') = \langle A_i(t)B_j(t')\rangle - \langle A_i(t)\rangle\langle B_j(t')\rangle, \tag{14}$$

where $r = |j - i|$ is the relative distance. Furthermore, we denote the spatial Fourier transform of the correlation function $C_r^{AB}(t, t')$ as

$$\tilde{C}_q^{AB}(t, t') = \sum_{r=0}^{L-1} C_r^{AB}(t, t')e^{iqr}, \tag{15}$$

where $q = 2\pi k/L$ and $k = 0, 1, \ldots, L-1$ and the inverse Fourier transform is

$$C_r^{AB}(t, t') = \frac{1}{L}\sum_q \tilde{C}_q^{AB}(t, t')e^{-iqr}. \tag{16}$$

By introducing a truncation scheme as discussed below, we can theoretically compute the statistics of different combinations of various local currents $\mathcal{J}_i$, $\mathcal{J}_i^{(d)}$, $\mathcal{J}_i^{(fl)}$ as well as mass m_i, essentially in terms of the following two correlation functions: $\langle \mathcal{Q}_i(t)\mathcal{Q}_j(t')\rangle$ and $\langle m_i(t)\mathcal{Q}_j(t')\rangle$.

B. Theory

For the conserved Manna sandpile, we write the stochastic update equation of the integrated current $\mathcal{Q}_i(t)$ in an infinitesimal time (continuous) interval $[t, t+dt]$,

$$\mathcal{Q}_i(t+dt) = \begin{cases} \textit{events} & \textit{probabilities} \\ \mathcal{Q}_i(t)+1 & \frac{1}{2}\hat{a}_i(t)dt \\ \mathcal{Q}_i(t)+2 & \frac{1}{4}\hat{a}_i(t)dt \\ \mathcal{Q}_i(t)-1 & \frac{1}{2}\hat{a}_{i+1}(t)dt \\ \mathcal{Q}_i(t)-2 & \frac{1}{4}\hat{a}_{i+1}(t)dt \\ \mathcal{Q}_i(t) & 1-\Sigma dt, \end{cases} \tag{17}$$

where $\Sigma = [\hat{a}_i(t) - \hat{a}_{i+1}(t)]$. Using the above update rules, the time-evolution equation for the first moment of the time-integrated current $\mathcal{Q}_i(t)$ can be written as

$$\frac{d}{dt}\langle \mathcal{Q}_i(t)\rangle = \langle \hat{a}_i(t)\rangle - \langle \hat{a}_{i+1}(t)\rangle. \tag{18}$$

Similarly, using Eq. (17), we find the time-evolution equation for the second moment $\langle \mathcal{Q}_i(t)\mathcal{Q}_{i+r}(t')\rangle = C_r^{\mathcal{Q}\mathcal{Q}}(t, t')$ of the integrated current at two different times t and t', for $t > t'$, as given below (see Appendix C 1 for details),

$$\frac{d}{dt}C_r^{\mathcal{Q}\mathcal{Q}}(t, t') = \left[C_r^{\hat{a}\mathcal{Q}}(t, t') - C_{r-1}^{\hat{a}\mathcal{Q}}(t, t')\right]. \tag{19}$$

The above equation, which is central to our study, is however difficult to solve exactly due to an infinite hierarchy of correlation functions involved and so we employ below an approximation scheme.

We note that the evolution of space and time-dependent activity-current correlation function $C_r^{\hat{a}\mathcal{Q}}(t, t')$ appearing in Eq. (19) contains higher-order correlation functions, involving activity, current, and some other observables. The calculations of the higher-order correlations would eventually result in a rapidly growing complexity in the hierarchy of correlation functions, which do not constitute a closed set of equations. More specifically, one can start with the infinitesimal time

update equation for $\hat{a}_i$ itself,

$$\hat{a}_i(t+dt) = \begin{cases} \textit{events} & \textit{probabilities} \\ \hat{a}_i(t)+1 & \frac{1}{2}\hat{a}_{i+1}(t)\hat{p}_i(t)\delta_{m_i,1}dt \\ \hat{a}_i(t)+1 & \frac{1}{2}\hat{a}_{i-1}(t)\hat{p}_i(t)\delta_{m_i,1}dt \\ \hat{a}_i(t)+1 & \frac{1}{4}\hat{a}_{i+1}(t)\hat{p}_i(t)dt \\ \hat{a}_i(t)+1 & \frac{1}{4}\hat{a}_{i-1}(t)\hat{p}_i(t)dt \\ \hat{a}_i(t)-1 & \hat{a}_i(t)(\delta_{m_i,2}+\delta_{m_i,3})dt \\ \hat{a}_i(t) & 1-\Sigma dt, \end{cases} \tag{20}$$

where $\hat{p}_i(t) = [1-\hat{a}_i(t)]$ and $\Sigma = [\hat{p}_i(t)/2](\delta_{m_i,1} + 1/2)[\hat{a}_{i+1}+\hat{a}_{i-1}] + \hat{a}_i(\delta_{m_i,2}+\delta_{m_i,3})$. From this update equation, for $t > t'$, we can write the evolution equation for $C_r^{a\mathcal{Q}}(t,t')$ as

$$\frac{d}{dt}C_r^{a\mathcal{Q}}(t,t') \equiv \frac{d}{dt}\langle \hat{a}_0(t)\mathcal{Q}_r(t')\rangle_c = \left\langle \left\{ \frac{d}{dt}\hat{a}_0(t) \right\} \mathcal{Q}_r(t') \right\rangle_c, \tag{21}$$

where the observable inside the curly bracket evolves according to the equation

$$\frac{d}{dt}\hat{a}_0(t) = -\hat{a}_0(t)(\delta_{m_0,2}+\delta_{m_0,3}) + \{\hat{p}_0(t)[\hat{a}_1(t)+\hat{a}_{L-1}(t)]\}\left(\frac{1}{2}\delta_{m_0,1}+\frac{1}{4}\right). \tag{22}$$

Clearly, to solve for $C_r^{a\mathcal{Q}}(t,t')$, one needs to calculate the correlation functions $\langle \delta_{m_0,2}\hat{a}_0(t)\mathcal{Q}_r(t')\rangle$ and $\langle \delta_{m_0,1}\hat{a}_0(t)\hat{a}_1(t)\mathcal{Q}_r(t')\rangle$, which would in turn involve another set of even higher-order correlation functions; of course, in this way, one generates an infinite hierarchy of equations, which is difficult to handle.

We bypass the difficulty by employing the following approximation scheme, which in fact truncates the otherwise infinite hierarchy: To this end, we approximate the local diffusive current, which is the gradient of the instantaneous local activity and is written as

$$\mathcal{J}_i^{(d)}(t) = [\hat{a}_i(t) - \hat{a}_{i+1}(t)] \equiv D(\bar{\rho})[m_i(t) - m_{i+1}(t)], \tag{23}$$

where the bulk-diffusion coefficient is given by $D(\bar{\rho}) = a'(\bar{\rho})$ as in Eq. (7) and can be treated as a constant. Essentially, we have assumed in the above truncation scheme that fluctuations around the global density $\bar{\rho}$ are small and the local current (the gradient of activity) relaxes diffusively via the gradient of local mass. As demonstrated later, this approximation captures relevant correlations quite well on the large (hydrodynamic) timescales. More specifically, to compute correlations between any observable $A(t)$ (e.g., current or mass) and the current observable $\mathcal{J}_i^{(d)}(t)$, we replace the diffusive-current observable $\mathcal{J}_i^{(d)}(t)$ by its truncated form as given on the right-hand side of Eq. (23), to obtain the following equality (approximate):

$$\langle A(t)\mathcal{J}_i^{(d)}(t')\rangle \simeq a'(\bar{\rho})[A(t)\{m_i(t') - m_{i+1}(t')\}]. \tag{24}$$

Now we can proceed further by first rewriting Eq. (19) as

$$\frac{d}{dt}C_r^{\mathcal{Q}\mathcal{Q}}(t,t') = a'(\bar{\rho})\left[C_r^{m\mathcal{Q}}(t,t') - C_{r-1}^{m\mathcal{Q}}(t,t')\right], \tag{25}$$

and then expressing the time-evolution equation for the mass-current correlations $C_r^{m\mathcal{Q}}(t,t') = \langle m_i(t)\mathcal{Q}_{i+r}(t')\rangle - \langle m_i(t)\rangle\langle \mathcal{Q}_{i+r}(t')\rangle$ as

$$\frac{d}{dt}C_r^{m\mathcal{Q}}(t,t') \simeq a'(\bar{\rho})\sum_k \Delta_{r,k}C_k^{m\mathcal{Q}}(t,t'), \tag{26}$$

where have used Eq. (23) in the intermediate steps (see Appendix C 2). It is worth noting that, in Eq. (23) or in Eqs. (25) and (26), the activity appears simply as a global density-dependent constant prefactor $a(\bar{\rho})$ and thus we obtain a closed set of equations, involving only mass and current correlations. Equations (25) and (26) can be solved, albeit in terms of the activity $a(\bar{\rho})$, which however remains undetermined in our theory. Interestingly, it was previously possible to exactly calculate the dynamic correlation functions in simple exclusion processes [52] because, in that case, one already gets a closed set of equations for mass and current correlations and, furthermore, because the steady-state measure is a product one, allowing one to calculate various static (time-independent) quantities, which enter into the expression of the current and mass fluctuations. Without an explicit knowledge of the steady-state measure [53], the Manna sandpile, on the other hand, is nontrivial due to the nonzero spatial correlations present in the system, making explicit calculations of the static quantities, such as the density-dependent activity, quite difficult. Nevertheless, as shown below, by extending the formalism developed in the context of simple exclusion processes [52], one can calculate various dynamic correlations in terms of activity and obtain fluctuation relations, which precisely quantify the underlying relationship between dynamic and static fluctuations in the system.

At this stage, it is useful to introduce the Fourier representation of the respective correlation functions as given in Eq. (15), and we can then write Eqs. (25) and (26) in the respective Fourier modes,

$$\frac{d}{dt}\tilde{C}_q^{\mathcal{Q}\mathcal{Q}}(t,t') = a'(\bar{\rho})\tilde{C}_q^{m\mathcal{Q}}(t,t')[1-e^{iq}], \tag{27}$$

and

$$\frac{d}{dt}\tilde{C}_q^{m\mathcal{Q}}(t,t') = -a'(\bar{\rho})\lambda_q\tilde{C}_q^{m\mathcal{Q}}(t,t'), \tag{28}$$

where

$$\lambda_q = 2[1-\cos q]. \tag{29}$$

Now, Eqs. (27) and (28) can be integrated to have

$$\tilde{C}_q^{\mathcal{Q}\mathcal{Q}}(t,t') = \int_{t'}^{t} dt'' a'(\bar{\rho})\tilde{C}_q^{m\mathcal{Q}}(t'',t')[1-e^{iq}] + \tilde{C}_q^{\mathcal{Q}\mathcal{Q}}(t',t'), \tag{30}$$

and

$$\tilde{C}_q^{m\mathcal{Q}}(t,t') = e^{-a'(\bar{\rho})\lambda_q(t-t')}\tilde{C}_q^{m\mathcal{Q}}(t',t'). \tag{31}$$

respectively. However, to fully solve for the unequal-time correlation functions $\tilde{C}_q^{\mathcal{Q}\mathcal{Q}}(t,t')$ and $\tilde{C}_q^{m\mathcal{Q}}(t,t')$, we need to calculate their respective equal-time counterparts as well. First we obtain the evolution equation for the equal-time mass-current correlation function $C_r^{m\mathcal{Q}}(t',t')$ and then writing $C_r^{m\mathcal{Q}}(t',t')$ in the Fourier space [using Eq. (C9); see

Appendix C 4 for details], we get

$$\frac{d}{dt'}\tilde{C}_q^{m\mathcal{Q}}(t',t') = -a'(\bar{\rho})\lambda_q \tilde{C}_q^{m\mathcal{Q}}(t',t') + \tilde{f}_q(t'), \tag{32}$$

where the Fourier transform of the source term $\tilde{f}_q(t')$ in the steady state is given by

$$\tilde{f}_q = \tilde{C}_q^{m\hat{a}}(1-e^{-iq}) - 2a(\bar{\rho})(1-e^{-iq})\left[1+\frac{\lambda_q}{4}\right]. \tag{33}$$

Now Eq. (32) can be directly integrated to obtain

$$\tilde{C}_q^{m\mathcal{Q}}(t',t') = \int_0^{t'} dt'' e^{-a'(\bar{\rho})\lambda_q(t'-t'')}\tilde{f}_q(t''), \tag{34}$$

substituting which into Eq. (31), we get the unequal-time mass-current correlation function in terms of $\tilde{f}_q$,

$$\tilde{C}_q^{m\mathcal{Q}}(t,t') = \int_0^{t'} dt'' e^{-a'(\bar{\rho})\lambda_q(t-t'')}\tilde{f}_q(t''). \tag{35}$$

To calculate the above correlation, we need to calculate the activity-mass correlation as in Eq. (33). Importantly, as shown below, we can calculate the static (time-independent) activity-mass correlation function exactly in the steady state (see Appendix C 5). Using the steady-state condition $dC_r^{mm}(t,t)/dt = 0$, we obtain

$$\frac{d}{dt}C_r^{mm}(t,t) = \sum_k 2\langle m_0 \Delta_{rk}\hat{a}_k\rangle_c + B_r = 0, \tag{36}$$

where B_r is the source term having the form

$$B_r(\bar{\rho}) = 7a(\bar{\rho})\delta_{0,r} - 4a(\bar{\rho})(\delta_{0,r+1}+\delta_{0,r-1}) + \frac{a(\bar{\rho})}{2}(\delta_{0,r+2}+\delta_{0,r-2}). \tag{37}$$

Equation (36) can be solved by employing a generating function,

$$G(z) = \sum_{r=0}^{\infty} C_r^{m\hat{a}} z^r, \tag{38}$$

for the equal-time mass-activity correlation; see Appendix (C 5). Here we directly provide the solution of the generating function in terms of the static density-dependent activity,

$$G(z) = \frac{3a(\bar{\rho})}{2} - \frac{a(\bar{\rho})}{4}z, \tag{39}$$

implying the mass-activity static correlation to be

$$C_r^{m\hat{a}} = \begin{cases} \frac{3a(\bar{\rho})}{2} & \text{for } r=0 \\ -\frac{a(\bar{\rho})}{4} & \text{for } |r|=1 \\ 0 & \text{otherwise,} \end{cases} \tag{40}$$

which is in fact exact. Then, by writing the Fourier transform of the above equation, we have

$$\tilde{C}_q^{m\hat{a}} = a(\bar{\rho}) + \frac{a(\bar{\rho})}{4}\lambda_q, \tag{41}$$

and substituting the above in Eq. (33), we straightforwardly obtain

$$\tilde{f}_q = -a(\bar{\rho})(1-e^{-iq})\left(1+\frac{\lambda_q}{4}\right). \tag{42}$$

C. Time-integrated current fluctuation

In this section, we calculate the time-integrated bond-current fluctuation by using the theory developed in the previous section. To this end, we substitute Eq. (42) into Eq. (35) and get an explicit solution the first term on the right-hand side of Eq. (30). Similarly, we can calculate the second term on the right-hand side of Eq. (30) as given below:

$$C_r^{\mathcal{Q}\mathcal{Q}}(t,t) \simeq \int_0^t dt'\Gamma_r(t') + \frac{1}{L}\int_0^t dt' a'(\bar{\rho}) \times \sum_{q=0}^{L-1}\tilde{C}_q^{m\mathcal{Q}}(t',t')[1-e^{iq}](2-\lambda_{qr}), \tag{43}$$

where $\lambda_{qr} = 2[1-\cos(qr)]$; see Appendix C 3 for details. Here the quantity $\Gamma_r(t)$ is the strength of the steady-state correlation function for the fluctuating current $\langle \mathcal{J}_0^{(fl)}(t)\mathcal{J}_r^{(fl)}(t')\rangle = \Gamma_r(t)\delta(t-t')$ as derived later in Eq. (59). Since we are interested only in the steady-state properties, the strength Γ_r is replaced by its steady-state value,

$$\Gamma_r(\bar{\rho}) = 3a(\bar{\rho})\delta_{0,r} - \frac{a(\bar{\rho})}{2}(\delta_{0,r+1}+\delta_{0,r-1}), \tag{44}$$

which depends on global density $\bar{\rho}$ through the density-dependent activity $a(\bar{\rho})$; for the detailed calculation of the strength Γ_r, see Sec. II D 1. Now the Fourier transform of Eq. (43) leads to the second term of right-hand side of Eq. (30). By using the inverse Fourier transform of Eq. (30), we finally obtain the desired space- and time-dependent current correlation function in the steady state:

$$C_r^{\mathcal{Q}\mathcal{Q}}(t,t') = t'\Gamma_r - a'(\bar{\rho})a(\bar{\rho})\frac{1}{L}\sum_q \int_0^{t'} dt'' \int_0^{t''} dt''' e^{-a'(\bar{\rho})\lambda_q(t''-t''')}\lambda_q\left(1+\frac{\lambda_q}{4}\right)(2-\lambda_{qr}) - a'(\bar{\rho})a(\bar{\rho})\frac{1}{L}\sum_q \int_{t'}^{t} dt'' \int_0^{t'} dt''' e^{-a'(\bar{\rho})\lambda_q(t''-t''')}\lambda_q\left(1+\frac{\lambda_q}{4}\right)e^{-iqr}. \tag{45}$$

The asymptotic behavior of the above equation can be straightforwardly obtained as given below (see Appendix B 1 for details):

$$\langle \mathcal{Q}^2(T)\rangle \simeq \begin{cases} \frac{2a(\bar{\rho})}{\sqrt{\pi a'(\bar{\rho})}}T^{\frac{1}{2}} & \text{for } 1 \ll T \ll L^2 \\ \frac{2a(\bar{\rho})}{L}T & \text{for } T \gg L^2. \end{cases} \tag{46}$$

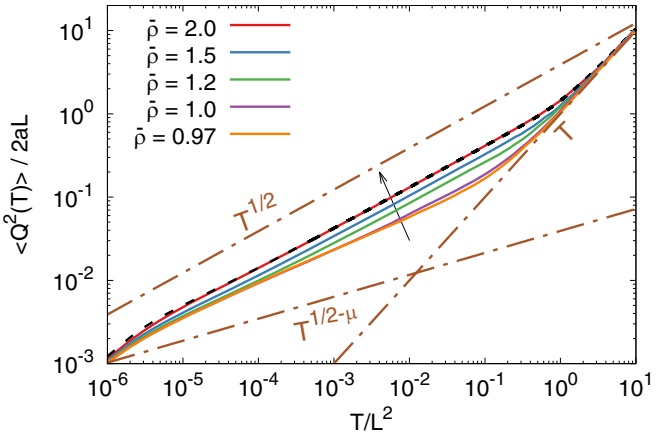

FIG. 1. Scaled fluctuations of cumulative (time-integrated) bond-current up to time T, obtained from simulations (solid lines), is plotted as a function of scaled time T/L^2 for different densities $\bar\rho = 2.0$ (red), $\bar\rho = 1.5$ (blue), $\bar\rho = 1.2$ (green), $\bar\rho = 1.0$ (purple), $\bar\rho = 0.97$ (orange), and for system size $L = 1000$, where the arrow across the solid lines denotes the increasing order of $\bar\rho$. Theory as in Eq. (45) with $r = 0, t = t' = T$ (black dashed line) is in excellent agreement with the simulation for $\bar\rho = 2.0$. Three guiding dot-dashed lines signify the initial-time subdiffusive growth $\langle Q^2(T)\rangle \sim T^{1/2}$ [as in the first part of Eq. (46)] and the late-time diffusive growth $\langle Q^2(T)\rangle \sim T$ [as in the second part of Eq. (46)] away from criticality, and the initial-time anomalously suppressed subdiffusive growth $\langle Q^2(T)\rangle \sim T^{1/2-\mu}$ [as in Eq. (48)] near criticality.

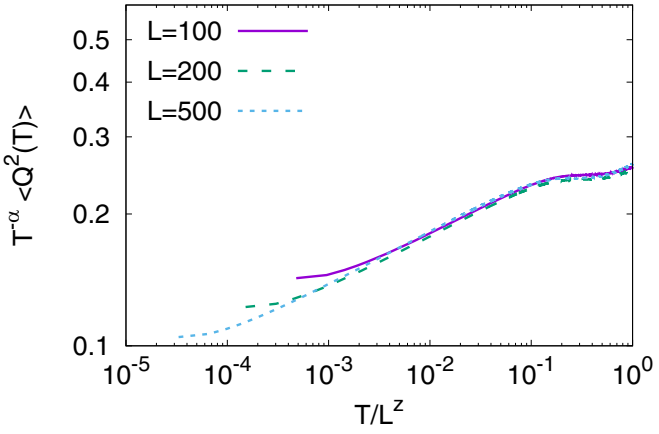

FIG. 2. The scaled variance $T^{-\alpha}\langle \mathcal{Q}^2(T)\rangle$ of time-integrated bond current $\mathcal{Q}(T)$ up to time T, obtained from simulations, is plotted as a function of scaled time T/L^z for system size $L = 100$ (solid magenta line), $L = 200$ (green dashed line), and $L = 500$ (blue dotted line) and for (near-critical) density $\bar\rho = 0.95$, where, to achieve the scaling collapse, we use $\alpha \approx 0.297$ and $z \approx 1.66$. The value of $\alpha \approx 0.297$ obtained from simulations is not far from $\alpha \approx 0.26$ obtained from theory as in Eqs. (47) and (48) with $\beta \approx 0.42$, $\nu_\perp \approx 1.81$ [21].

In the simulation, we verify a special case of Eq. (45) by putting $r = 0$ and $t = t' \equiv T$, i.e., the time-integrated bond current fluctuation $\langle \mathcal{Q}^2(T)\rangle \equiv C_0^{\mathcal{Q}\mathcal{Q}}(T, T)$ (here average current $\langle \mathcal{Q}(T)\rangle = 0$ for the steady-state measurement). In Fig. 1, we plot $\langle Q^2(T)\rangle$, obtained from the simulation (plotted in solid lines), for various densities $\bar\rho = 2.0$ (red), $\bar\rho = 1.5$ (blue), $\bar\rho = 1.2$ (green), $\bar\rho = 1.0$ (purple), $\bar\rho = 0.97$ (orange) as a function of T. The arrow across the solid lines in the Fig. 1 signifies the increasing order of global density $\bar\rho$.

Indeed the dynamical behaviors as predicted by the asymptotics in Eq. (46) are different in two different time regimes: On smaller initial timescales $1 \ll T \ll L^2$, the time-integrated current grows subdiffusively as $T^{1/2}$ and, on larger (hydrodynamic) timescales $T \gg L^2$, grows linearly as T. We compare the simulation result with that obtained from our theory (45) with $r = 0$ and $t = t' = T$ for $\bar\rho = 2.0$ (black dashed line) and for system size $L = 1000$; one can see an excellent agreement between simulation and theory.

As mentioned previously, our theory is expected to be valid at hydrodynamic times ($T \gg L^z$) and the small-time ($T \ll L^z$) behavior of current fluctuation, especially near criticality, is not quite well captured by Eq. (45). However the small-time behavior near criticality can still be obtained qualitatively by using the following standard scaling analysis. Indeed, first resorting to a simple dimensional analysis, we can see that the activity scales as $a(\Delta) \sim \Delta^\beta \sim T^{-\beta/\nu_\perp z}$, where the relative density $\Delta = \bar\rho - \rho_c \ll 1$ and we use the following scaling relations: correlation length $\xi \sim T^{1/z}$ the relative density $\Delta \sim \xi^{-1/\nu_\perp} \sim T^{-1/\nu_\perp z}$, with z being the dynamic exponent. Thus, by writing $a(\Delta)/[a'(\Delta)]^{1/2} \sim T^{-\mu}$, we straightforwardly have, in the initial-time regime $1 \ll T \ll L^z$, the scaling behavior of the current fluctuation $\langle \mathcal{Q}^2(T)\rangle \sim [a/(a')^{1/2}]T^{1/2} \sim T^\alpha$, where the exponents

$$\alpha = \tfrac{1}{2} - \mu \tag{47}$$

and

$$\mu = \frac{\beta + 1}{2\nu_\perp z}. \tag{48}$$

More precisely, near criticality we expect the following scaling form for the time-integrated bond-current fluctuation to hold,

$$\langle \mathcal{Q}^2(T)\rangle \simeq L^{\alpha z}\mathcal{G}\left(\Delta L^{1/\nu_\perp}, \frac{T}{L^z}\right) = T^\alpha \mathcal{F}\left(\Delta L^{1/\nu_\perp}, \frac{T}{L^z}\right), \tag{49}$$

where $\mathcal{G}$ and $\mathcal{F}$ are two scaling functions. To determine the exponent α in Eq. (49) from simulations, we take density value such that $\Delta L^{1/\nu_\perp} \to 0$ and then we plot in Fig. 2 the scaled variance of time-integrated bond current $T^{-\alpha}\langle \mathcal{Q}^2(T)\rangle$ as a function of the scaled time T/L^z for rather quite smaller system sizes $L = 100$ (solid magenta line), $L = 200$ (green dashed line), and $L = 500$ (blue dotted line), respectively, and for $\bar\rho = 0.95$. We get a reasonably good scaling collapse of simulation data, with the exponent estimated to be $\alpha \approx 0.297$; our theoretical prediction of the exponent $\alpha \approx 0.26$, computed from scaling relations Eqs. (47) and (48) by using $\beta \approx 0.42$, $z \approx 1.66$, and $\nu_\perp \approx 1.81$ [21], slightly underestimates that obtained from simulation though.

The variance of time-integrated bond current is known to grow subdiffusively in the initial-time regime in diffusive systems, such as symmetric simple exclusion processes [52,54]. Now, away from criticality, the relaxation processes in sandpiles are diffusive [41,42] and, therefore not surprisingly, the current fluctuation exhibits a subdiffusive growth, as derived in the first part of Eq. (46). Near-critical relaxation processes

in the Manna sandpile, on the other hand, are anomalous and we observe nontrivial scaling behavior. When compared with a normal diffusive system, the Manna sandpile near criticality exhibits strong suppression of current fluctuations and much slower subdiffusive growth of temporal fluctuations due to the lack of local activity, as described in Eq. (49); we call it a "dynamic hyperuniformity," which is quite analogous to hyperuniformity studied in the spatial domain [33,35] and is reminiscent of that identified in the context of temporal statistics of avalanches in a particular version sandpile, called the Oslo rice pile [46]. Of course, the dynamic hyperuniformity, or the anomalously subdiffusive growth of temporal fluctuations, can be equivalently characterized in terms of the current and mass power spectra, or the respective dynamic correlation functions, as discussed in the following sections.

D. Current fluctuation and its power spectrum

1. Instantaneous current

In this section, we calculate in the steady-state the time-dependent (unequal-time) current-current correlation function $C_r^{\mathcal{J}\mathcal{J}}(t) \equiv C_r^{\mathcal{J}\mathcal{J}}(t, t' = 0)$ of the instantaneous bond current by taking time derivative of time-integrated bond current correlation as given below,

$$C_r^{\mathcal{J}\mathcal{J}}(t) = \left[\frac{d}{dt}\frac{d}{dt'}C_r^{\mathcal{Q}\mathcal{Q}}(t, t')\right]_{t'=0}, \tag{50}$$

where $t \geqslant t'$. Now, after differentiating Eq. (45), we can write the time-dependent current correlation as

$$C_r^{\mathcal{J}\mathcal{J}}(t) = \Gamma_r \delta(t) - a'(\bar{\rho})a(\bar{\rho})\left[\frac{1}{L}\sum_q e^{-a'(\bar{\rho})\lambda_q t}\lambda_q\left(1 + \frac{\lambda_q}{4}\right)e^{-iqr}\right], \tag{51}$$

where Γ_r is the strength of the fluctuating current $\mathcal{J}^{fl}(t)$ and calculated below [see Eq. (59)]. We note that, as $\lambda_q \geqslant 0$ for any q, the current correlation function is *negative* $C_r^{\mathcal{J}\mathcal{J}}(t) < 0$ for any $t > 0$. Moreover, provided that we first take the infinite-system-size limit $L \to \infty$, the time-integrated bond current correlation function $C_0^{\mathcal{J}\mathcal{J}}(t)$ over a large time interval $[-T, T]$ decays as a function of time T as given below,

$$\int_{-T}^{T} C_0^{\mathcal{J}\mathcal{J}}(t)dt \simeq \frac{a(\bar{\rho})}{\sqrt{\pi a'(\bar{\rho})}}T^{-\frac{1}{2}}. \tag{52}$$

Finally, by taking the limit $T \to \infty$, we obtain the following identity:

$$\int_{-\infty}^{\infty} C_0^{\mathcal{J}\mathcal{J}}(t)dt = 0, \tag{53}$$

see Appendix B 2 for details. Indeed, the above result is a direct consequence of the negative current correlation present in the system and explains why the time-integrated bond current fluctuation, as derived in Eq. (46), grows subdiffusively in the initial-time regime $1 \ll t \ll L^2$. The asymptotic form of the time-dependent instantaneous current correlation function, for $t > 0$, in the thermodynamic limit can be written as

$$C_0^{\mathcal{J}\mathcal{J}}(t) \simeq -\frac{a(\bar{\rho})}{4\sqrt{\pi a'(\bar{\rho})}}t^{-\frac{3}{2}}, \tag{54}$$

where the density-dependent term $a(\bar{\rho})/[a'(\bar{\rho})]^{1/2}$ in the prefactor is the same as that in Eq. (46) (see Appendix B 2). Again, by employing the dimensional scaling argument used in the previous section to derive Eq. (48), we obtain a modified power-law decay of the instantaneous current correlation near criticality,

$$C_0^{\mathcal{J}\mathcal{J}}(t) \sim -t^{-\left(\frac{3}{2}+\mu\right)}. \tag{55}$$

Clearly the decay is faster than that away from criticality. As discussed previously, the faster decay of the near-critical current correlation function is due to the fact that the activity is very small in the vicinity of criticality, thus resulting in the anomalous suppression of fluctuations. Indeed the suppressed fluctuation is characterized by the exponent $\mu > 0$, whereas $\mu = 0$ signifies the subdiffusive growth of the time-integrated current, expected in a normal diffusive system.

2. Fluctuating current

Now we discuss the dynamic properties of the fluctuating part $\mathcal{J}_i^{(fl)}(t)$ in the instantaneous bond current, which has already been defined in Eq. (12) and whose strength appears in the actual current correlation functions [e.g., see Eqs. (52) and (50)]. Here we derive the general space and time dependence of the correlation function $C_r^{\mathcal{J}^{(fl)}\mathcal{J}^{(fl)}}(t, t')$ of the fluctuating current $\mathcal{J}_i^{(fl)}(t)$ by using the relation [obtained from the definition in Eq. (12)]

$$C_r^{\mathcal{J}^{(fl)}\mathcal{J}^{(fl)}}(t, 0) = C_r^{\mathcal{J}\mathcal{J}}(t, 0) - C_r^{\mathcal{J}\mathcal{J}^{(d)}}(t, 0) - C_r^{\mathcal{J}^{(d)}\mathcal{J}}(t, 0) + C_r^{\mathcal{J}^{(d)}\mathcal{J}^{(d)}}(t, 0), \tag{56}$$

and a second relation

$$C_r^{\mathcal{J}\mathcal{J}^{(d)}}(t, 0) \equiv \frac{d}{dt}C_r^{\mathcal{Q}\mathcal{J}^{(d)}}(t, 0) = C_r^{\mathcal{J}^{(d)}\mathcal{J}^{(d)}}(t, 0). \tag{57}$$

We see that the second and the fourth terms of Eq. (56) cancel each other. Again, by using the following relation, for $t > t'$,

$$C_r^{\mathcal{J}^{(d)}\mathcal{J}}(t, t') = \frac{d}{dt'}C_r^{\mathcal{J}^{(d)}\mathcal{Q}}(t, t') = \frac{d}{dt'}\frac{d}{dt}C_r^{\mathcal{Q}\mathcal{Q}}(t, t'), \tag{58}$$

in Eq. (56) along with $t' = 0$, we finally have the time-dependent correlation function for the fluctuating current,

$$C_r^{\mathcal{J}^{(fl)}\mathcal{J}^{(fl)}}(t, t' = 0) \equiv C_r^{\mathcal{J}^{(fl)}\mathcal{J}^{(fl)}}(t) = \delta(t)\Gamma_r(\bar{\rho}), \tag{59}$$

where $\Gamma_r(\bar{\rho})$ is the density-dependent strength of the fluctuating current $\mathcal{J}^{(fl)}$.

The analytical expression of the strength Γ_r as given in Eq. (44) has some interesting properties, which are due to the two-particle transfer rule in the Manna sandpile and are noticeably different from that in the variant of sandpile with one-particle transfer [55] and symmetric simple exclusion processes studied in Ref. [52]. As in the simple exclusion processes, the strength Γ_r for the sandpile with one-particle transfer rule can be shown to be simply delta correlated in space, i.e., $\Gamma_r = 2a(\bar{\rho})\delta_{r,0}$ [56]; this is because both the models have a steady state with a product measure and therefore do not have any spatial correlations. But, in the case of the Manna

sandpile, there are nonzero spatial correlations, leading to the spatially correlated fluctuating current, i.e., $\Gamma_r \neq 0$ for $r \neq 0$, as shown in Eq. (44). Indeed, as our calculation shows (for details, see Appendix C 3), Eq. (44) is exact in the case of Manna sandpile and we have

$$\Gamma_0 = 3a(\bar{\rho}), \tag{60}$$

being the strength of the fluctuating current $\mathcal{J}_i^{(fl)}$ across a single bond $(i, i+1)$. Moreover, we find that there exists a sum rule

$$\sum_r \Gamma_r = 2a(\bar{\rho}), \tag{61}$$

which, as shown later in Eq. (69), is directly related to the scaled space-time integrated current fluctuations and therefore related to another transport coefficient, called the mobility, or equivalently, the conductivity, defined as the ratio between average current and an externally applied small biasing force [41,51]. It has been derived in Ref. [41] that the conductivity in the Manna sandpile is nothing but the density-dependent activity $a(\bar{\rho})$ itself. Remarkably, as shown in the next section, here we show that one can indeed relate the conductivity directly to the current fluctuation in the system.

To verify Eq. (59) in simulation, let us first define a cumulative (space-time integrated) fluctuating current across a subsystem of size l and up to time T,

$$\mathcal{Q}_l^{(fl)}(T) = \int_0^T dt \sum_{i=0}^{l-1} \mathcal{J}_i^{(fl)}(t). \tag{62}$$

Then, using Eqs. (44) and(59) and after some algebraic manipulations, we obtain, for $l < L$, a fluctuation relation, which immediately connects the scaled current fluctuation and the density-dependent activity,

$$\frac{1}{lT}\left\langle \left(\mathcal{Q}_l^{(fl)}(T)\right)^2 \right\rangle = 2a(\bar{\rho})\left(1 + \frac{1}{2l}\right). \tag{63}$$

In Fig. 3 (top panel), we plot the left-hand side of Eq. (63) as a function of the relative density $\Delta = \bar{\rho} - \rho_c$ for different subsystem sizes $l = 1$ (solid red line), $l = 2$ (solid blue line), $l = 5$ (solid green line), $l = 10$ (solid purple line); we take system size $L = 1000$ and final time $T = 100$. The arrow across the solid lines denotes the increasing order of the subsystem size l. Note that the variance of subsystem fluctuating current for subsystem size $l = 1$ is actually the strength Γ_0 of the fluctuating bond current; the corresponding analytical result $\Gamma_0 = 3a(\bar{\rho})$ (dashed black line) as in Eq. (60) shows an excellent agreement with simulations. For comparison, in the same Fig. 3 (top panel), we also plot $2a(\Delta)$ as a function of Δ (the brown dot-dashed line), to demonstrate that, as subsystem size l increases, the scaled variance [left-hand side of Eq. (63)] indeed converges towards $2a(\bar{\rho})$, as predicted in Eq. (63). To show this convergence more quantitatively, in Fig. 3 (bottom panel) we plot the scaled quantity $2l[\langle(\mathcal{Q}_l^{(fl)})^2\rangle - 2a]$ for various subsystem sizes $l = 1$ (red solid line), $l = 2$ (blue dashed line), $l = 5$ (green dotted line), and $l = 10$ (purple dot-dashed line); we see that all the curves collapse excellently onto each other and the collapsed master curve matches excellently with the analytically predicted value $2a(\Delta)$ derived in Eq. (63).

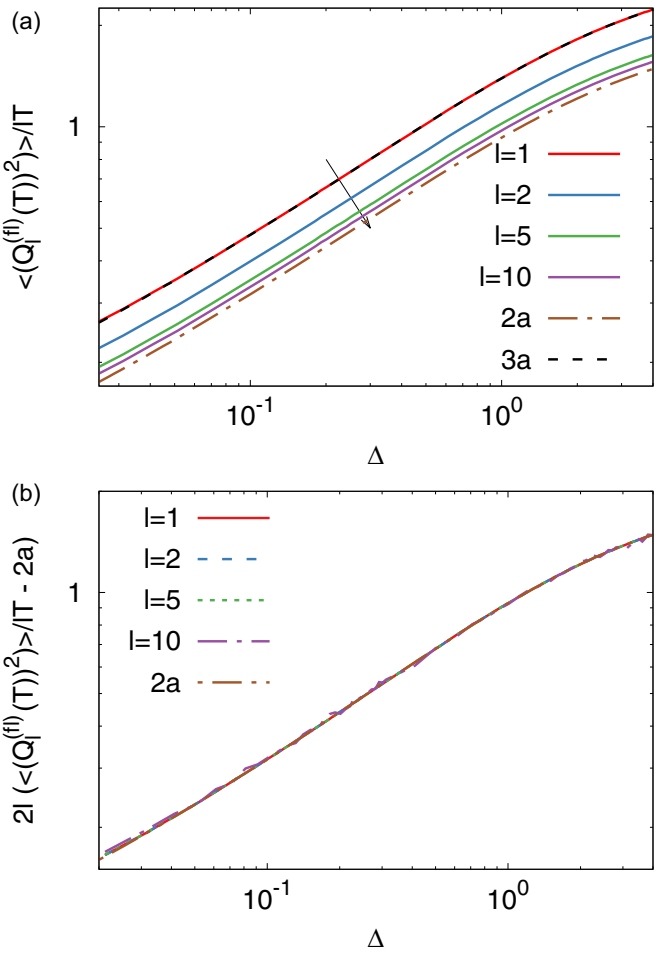

FIG. 3. (top panel) The scaled variance $\langle[\mathcal{Q}_l^{(fl)}(T)]^2\rangle/lT$ of space-time-integrated fluctuating current $\mathcal{Q}_l^{(fl)}(T)$ up to time T [as defined in Eq. (62)] obtained from simulations is plotted as a function of relative density Δ for different subsystem sizes $l = 1$ (solid red line), $l = 2$ (solid blue line), $l = 5$ (solid green line), $l = 10$ (solid purple line), and the arrow across the solid line denotes the increasing order of the subsystem size l; we have used system size $L = 1000$ and final time $T = 1000$. The theoretical prediction as in Eq. (63) with $l = 1$ (black dashed line) is in excellent agreement with the corresponding simulation. Also, one can see that the variance for large l converges quite rapidly to the theoretically predicted value $2a(\bar{\rho})$ [i.e., Eq. (63) for $l \gg 1$] (brown dot-dashed line). (bottom panel) A scaling collapse of the scaled variance of space-time-integrated fluctuating current minus the asymptotic value $2a(\bar{\rho})$ for different subsystem sizes is observed when plotted as a function of relative density Δ, and it is in excellent agreement with theory [Eq. (63)].

3. Space-time integrated current

In this section we calculate the steady-state variance $\langle\bar{Q}^2(l,T)\rangle - \langle\bar{Q}(l,T)\rangle^2$ of the cumulative (space-time integrated) actual particle current $\bar{Q}(l,T) = \sum_{i=0}^{l-1} \mathcal{Q}_i(T)$ across a subsystem of size l and up to time T, which can be written as

$$\langle\bar{Q}^2(l,T)\rangle - \langle\bar{Q}(l,T)\rangle^2 = \langle\bar{Q}^2(l,T)\rangle$$
$$= lC_0^{\mathcal{Q}\mathcal{Q}}(T,T) + \sum_{r=1}^{l-1} 2(l-r)C_r^{\mathcal{Q}\mathcal{Q}}(T,T), \tag{64}$$

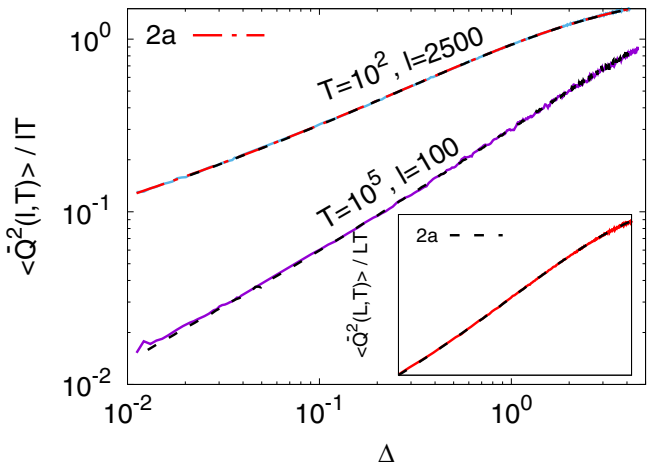

FIG. 4. Scaled space-time-integrated current fluctuations as a function of relative density. The simulation data for subsystem size $l = 2500$ and $T = 100$ is plotted on top in a *solid sky-blue line* and data for $l = 100$ and $T = 10^5$ is plotted at bottom in a *solid magenta line*. We compared the analytical result Eq. (66) (corresponding dashed black lines) with the simulation, which is in excellent agreement. Simulation data have been taken for $L = 5000$ in both cases. We note that the result for the larger subsystem size l and smaller T (upper solid line) almost coincide with twice the local activity, $2a(\Delta)$, as a function of Δ (red dot-dashed line). *In the inset* we compare the scaled total current fluctuation and twice the activity $2a(\bar{\rho})$ as a function of Δ.

where we have used the fact that the average steady-state current is zero, i.e., $\langle \bar{Q}(l,T)\rangle = 0$. Now, by using the following identity:

$$\sum_{r=1}^{l-1} 2(l-r)(2-\lambda_{rn}) = 2\left(\frac{\lambda_{ln} - l\lambda_n}{\lambda_n}\right), \tag{65}$$

we can rewrite Eq. (64) as

$$\begin{aligned}\left\langle \bar{Q}(l,T)^2 \right\rangle = {} & 2a(\bar{\rho})lT + a(\bar{\rho})T(1-\delta_{l,L}) - 2a(\bar{\rho})\frac{a'(\bar{\rho})}{L} \\ & \times \sum_q \frac{a'(\bar{\rho})\lambda_q T - 1 + \exp(-\lambda_q a'(\bar{\rho})T)}{(\lambda_q a'(\bar{\rho}))^2} \\ & \times \lambda_q\left(1+\frac{\lambda_q}{4}\right)\frac{\lambda_{ql}}{\lambda_q}.\end{aligned} \tag{66}$$

In Fig. 4, we plot the subsystem current fluctuation $\langle \bar{Q}^2(l,T)\rangle$ obtained from simulations as a function of relative density $\Delta = \rho - \rho_c$ for various subsystem sizes l and final times T: $l = 2500$, $T = 100$ (upper solid sky-blue line) and $l = 100$, $T = 10^5$ (lower solid magenta line). In the same figure we also compare the simulation results with theory Eq. (66): $l = 2500$, $T = 100$ and $l = 100$, $T = 10^5$ (both in black dashed line); we observe excellent agreement between simulations and theory. Here we note that the results for the larger subsystem size l and smaller T (upper solid line) almost coincide with twice the local activity, $2a(\Delta)$, as a function of Δ (red dot-dashed line).

Importantly, the asymptotic expression of the variance of the cumulative subsystem (space-time integrated) current as in Eq. (66) depends on the order of limits of the two variables $T \gg 1$ and $l \gg 1$, i.e.,

$$\frac{\langle \bar{Q}^2(l,T)\rangle}{lT} \simeq \begin{cases} \frac{2a(\bar{\rho})}{\sqrt{\pi a'(\bar{\rho})}}\frac{l}{\sqrt{T}} & \text{for } T \gg 1,\ l \gg 1 \\ 2a(\bar{\rho}) - \frac{8a(\bar{\rho})\sqrt{a'(\bar{\rho})}}{3\sqrt{\pi}}\frac{\sqrt{T}}{l} & \text{for } l \gg 1,\ T \gg 1, \end{cases} \tag{67}$$

see Appendix B 3 for details. The first expression in the above equation has been obtained by taking the limit in the following order, first $T \gg 1$ and then the limit $l \gg 1$. In this particular order of limits, the scaled fluctuation $\langle \bar{Q}^2(l,T)\rangle/lT$ decreases as $1/\sqrt{T}$ and eventually vanishes in the limit of $T \to \infty$. On the other hand, if we take the limit in the opposite order, $l \gg 1$ first and then $T \gg 1$, we obtain the second asymptotic expression in Eq. (67). That is, in the limit $l \to \infty$, the scaled subsystem-current fluctuation $\langle \bar{Q}^2(l,T)\rangle/lT$ tends to $2a(\bar{\rho})$ as one increases T,

$$\sigma_{\bar{Q}}^2(\bar{\rho}) \equiv \lim_{l\to\infty}\lim_{T\to\infty} \frac{\langle \bar{Q}^2(l,T)\rangle}{lT} = 2a(\bar{\rho}), \tag{68}$$

where the infinite-subsystem-size limit is taken first, and then the infinite-time limit. Note that, in all the above cases, we have taken the large system size limit $L/l \gg 1$ at the very beginning. In fact, one can immediately identify the right-hand side of Eq. (68) as the mobility (equivalently, the conductivity) for the Manna sandpile, as calculated in Ref. [41]. Indeed, Eq. (68) can be thought of as a nonequilibrium version of the celebrated Green-Kubo relations well known for equilibrium systems [57].

Interestingly, if we take $l = L \gg 1$, which corresponds to the bond currents summed over the whole system, we have the following identity:

$$\lim_{L\to\infty} \frac{\langle \bar{Q}^2(L,T)\rangle}{LT} = 2a(\rho) = \sum_r \Gamma_r. \tag{69}$$

Notably, the above equality is valid for any finite time T. This is because the sum of the diffusive currents over the full system, $\sum_{i=1}^{L} \mathcal{J}_i^{(d)}$, is zero by definition [see Eq. (13)]. Consequently the right-hand side of Eq. (69) is equal to the space-time integral of the fluctuating-current correlation function $\sum_{r=-\infty}^{\infty}\int_{-\infty}^{\infty} dt C_r^{\mathcal{J}^{(fl)}\mathcal{J}^{(fl)}}(t,0) = 2a(\bar{\rho})$, obtained using Eqs. (44), (59), and (61). In the inset of Fig. 4, the scaled variance $\langle \bar{Q}^2(L,T)\rangle/LT$ (solid red line) and twice the local activity $2a(\Delta)$ (black dashed line) are plotted as a function of Δ, which is in excellent agreement with Eq. (69). Clearly, below the critical point $\Delta < 0$, the system goes into an absorbing state and, as a result, the current fluctuation is identically zero. Usually activity is considered to be the order parameter in the sandpiles. Indeed, as the identity Eq. (69) suggests, the space-time integrated current fluctuation can serve as an order parameter and thus characterizes the dynamical state of the system. Later we show that the self-diffusion coefficient of tagged particles can be expressed in terms of the activity and, as previously noted in Ref. [27], it can be considered an alternative description of the system's order parameter.

4. Power spectrum

The two-point time-dependent correlation function for instantaneous bond current can be characterized also through the power spectrum analysis, which we perform in this section. From the *Wiener-Khinchin* theorem [58], the power spectrum for the instantaneous bond current $\mathcal{J}_i(t)$ is expressed in terms of the Fourier transform of the time-correlation functions,

$$S_{\mathcal{J}}(f) = \int_{-\infty}^{\infty} dt C_0^{\mathcal{J}\mathcal{J}}(t,0) e^{2\pi i f t}. \tag{70}$$

Setting $r = 0$ in Eq. (51), we perform the integration in the right-hand side of the above equation, leading to the following expression:

$$S_{\mathcal{J}}(f) = \frac{2a(\bar{\rho})}{L} + \frac{2a(\bar{\rho})}{L} \sum_q \left(1 + \frac{\lambda_q}{4}\right) \frac{4\pi^2 f^2}{\lambda_q^2 a'(\bar{\rho})^2 + 4\pi^2 f^2}. \tag{71}$$

Now, by subtracting the $f = 0$ mode

$$S_{\mathcal{J}}(0) = \lim_{T\to\infty} \frac{\langle \mathcal{Q}^2(T)\rangle}{T} = \frac{2a(\bar{\rho})}{L} \tag{72}$$

from the left-hand side of Eq. (71), we rewrite Eq. (71) in terms of the modified power spectrum $\tilde{S}_{\mathcal{J}}(f) = S_{\mathcal{J}}(f) - S_{\mathcal{J}}(0)$,

$$\tilde{S}_{\mathcal{J}}(f) = \frac{2a(\bar{\rho})}{L} \sum_q \left(1 + \frac{\lambda_q}{4}\right) \frac{4\pi^2 f^2}{\lambda_q^2 a'(\bar{\rho})^2 + 4\pi^2 f^2}. \tag{73}$$

We can now straightforwardly obtain the asymptotic form of Eq. (73) for small frequency $1/L^2 \ll f \ll 1$. To do this, we first replace the sum in Eq. (73) as an integral over the variable $x = q/2\pi$,

$$\tilde{S}_{\mathcal{J}}(f) \simeq 4a(\bar{\rho}) \int_{1/L}^{1/2} dx \frac{1 + \frac{\lambda(x)}{4}}{1 + \frac{\lambda^2(x) a'^2(\bar{\rho})}{4\pi^2 f^2}}, \tag{74}$$

where $\lambda(x) \simeq 4\pi^2 x^2$. Then, by performing the variable transformation

$$y = \frac{\lambda^2(x) a'^2(\bar{\rho})}{4\pi^2 f^2}, \tag{75}$$

and doing some algebraic manipulations, we immediately obtain the modified power spectrum of current,

$$\tilde{S}_{\mathcal{J}}(f) \simeq a(\bar{\rho}) \sqrt{\frac{f}{2\pi a'(\bar{\rho})}} \int_0^{\infty} dy \frac{y^{-\frac{3}{4}}}{(1+y)} = \frac{\sqrt{\pi} a(\bar{\rho})}{\sqrt{a'(\bar{\rho})}} f^{\frac{1}{2}}, \tag{76}$$

see Appendix A for details. Again, by using the previous dimensional scaling argument where $a/(a')^{1/2} \sim f^{\mu}$ with μ given in Eq. (48) (see Sec. II C), we obtain the desired scaling behavior of the subtracted power spectrum near criticality,

$$\tilde{S}_{\mathcal{J}}(f) \sim f^{\psi_{\mathcal{J}}}, \tag{77}$$

where $\psi_{\mathcal{J}} = 1/2 + \mu$. Since $\mu > 0$, with decreasing frequency, the near-critical power spectrum in the above equation (77) decays faster than that away from criticality [given by Eq. (76)]. In simulations, we calculate the power spectrum by discretizing time over a small interval δt and calculate the discrete Fourier transform

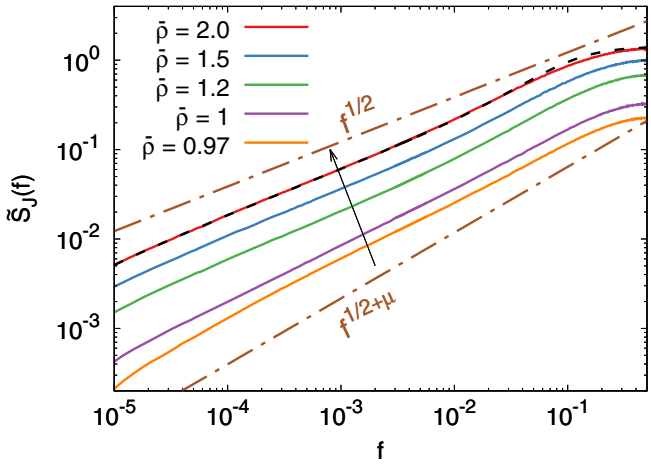

FIG. 5. Power spectrum of instantaneous current computed from simulations is plotted in solid lines as a function of frequency f for various densities $\rho = 2.0$ (red line), $\rho = 1.5$ (blue line), $\rho = 1.5$ (green line), $\rho = 1.0$ (purple line), $\rho = 0.97$ (orange line), and for system size $L = 1000$. The arrow across the solid lines signifies the incremental order of the density $\bar{\rho}$. The top and bottom dashed guiding lines represent the asymptotic behavior, the $f^{1/2}$ (far from criticality) and $f^{1/2+\mu}$ (near criticality) scaling, respectively, with $\mu \approx 0.24$, obtained by using $\beta \approx 0.42$, $\nu_{\perp} \approx 1.81$, and $z \approx 1.66$ in Eq. (48). The dashed black line represents the theoretical result Eq. (71) for $\rho = 2.0$ and is in excellent agreement with the corresponding simulation (top red solid line).

$$\tilde{\mathcal{J}}_{n;T} = \delta t \sum_{k=0}^{T-1} e^{i2\pi f_n k} \mathcal{J}_i(k), \tag{78}$$

where $f_n = n/T$ with T being large. Then we define the power spectrum of the bond current as

$$S_n = \lim_{T\to\infty} \frac{1}{T} \langle |\tilde{\mathcal{J}}_{n;T}|^2 \rangle. \tag{79}$$

In Fig. 5, we plot the subtracted power spectrum $\tilde{S}_{\mathcal{J}}(f)$ obtained from simulations in solid lines, for various densities $\rho = 2.0$ (red line), $\rho = 1.5$ (blue line), $\rho = 1.5$ (green line), $\rho = 1.0$ (purple line), and $\rho = 0.97$ (orange line). The arrow through the solid lines denotes the incremental order of the density $\bar{\rho}$. For $\rho = 2.0$, we also plot $\tilde{S}_{\mathcal{J}}(f)$ obtained from theory Eq. (73) (black dashed line), which shows an excellent agreement with simulation; top-most guiding line is $f^{1/2}$ [behavior away from criticality as in Eq. (76)] and the bottom-most guiding line is $f^{1/2+\mu}$ [behavior near criticality as in Eq. (77)].

E. Tagged-particle displacement fluctuation

In this section, we study the fluctuations in tagged particle displacements as a function of time. We can relate the sum of all individual time-integrated tagged particle displacement $\sum_{\alpha=1}^{N} X_{\alpha}(T)$, where the net displacement $X_{\alpha}(T)$ of the αth particle in a time interval $[0, T]$, to the space-time integrated

current by the following relation:

$$\sum_{\alpha=1}^{N} X_\alpha(T) = \sum_{i=0}^{L-1} \mathcal{Q}_i(T) = \bar{\mathcal{Q}}(L,T). \tag{80}$$

In the limit of large $T \gg L^2$, the self-diffusion coefficient $\mathcal{D}_s(\bar{\rho})$ can be defined through the mean-square tagged particle displacement of the αth particle as given below:

$$\langle X_\alpha^2(T)\rangle \simeq 2\mathcal{D}_s(\bar{\rho})T. \tag{81}$$

To compute the left-hand side of the above equation, we write the variance of the sum $\sum_{\alpha=1}^{N} X_\alpha(T)$ as

$$\left\langle \left[\sum_{\alpha=1}^{N} X_\alpha(T)\right]^2 \right\rangle = \sum_{\alpha,n}\sum_{\alpha',n'} \langle \delta X_\alpha(t_n)\delta X_{\alpha'}(t_{n'})\rangle = 2a(\bar{\rho})LT, \tag{82}$$

where $\delta X_\alpha(t)$ is the microscopic displacement of the αth particle in a small time interval $(t_n, t_n + \delta t)$:

$$X_\alpha(T) = \sum_n \delta X_\alpha(t_n), \tag{83}$$

and we have used Eq. (69) in the last line of Eq. (82). Now using $\langle \delta X_\alpha(t)\delta X_{\alpha'}(t')\rangle \simeq 0$ for $t \neq t'$ and therefore $\langle X_\alpha^2(T)\rangle = \sum_n \langle \delta X_\alpha^2(t_n)\rangle$, we get

$$\left\langle \left[\sum_{\alpha=1}^{N} X_\alpha(T)\right]^2 \right\rangle \simeq \sum_{\alpha=1}^{N} \langle X_\alpha^2(T)\rangle = N\langle X_\alpha^2(T)\rangle. \tag{84}$$

Comparing Eqs. (82), (81), and (84), we obtain the following relations,

$$\mathcal{D}_s(\bar{\rho}) = \frac{a(\bar{\rho})}{\bar{\rho}} = \frac{1}{\bar{\rho}}\left[\lim_{L,T\to\infty} \frac{\langle \bar{\mathcal{Q}}^2(L,T)\rangle}{2LT}\right], \tag{85}$$

which connects the self-diffusion coefficient, activity, and the space-time integrated current fluctuation. Alternatively, one can show the above relation using a slightly different argument as follows: First we note that $\langle X_\alpha^2(T)\rangle = \langle N_\alpha^{(h)}(T)\rangle$, where $N_\alpha^{(h)}(T)$ is the total number of hops, performed by the αth particle up to time T [27]. Summing over all particles we obtain

$$\sum_\alpha \langle X_\alpha^2(T)\rangle = \sum_\alpha \langle N_\alpha^{(h)}(T)\rangle = 2\langle N^{(tp)}(T)\rangle, \tag{86}$$

where $N^{(tp)}(T)$ is the total number of toppling in the whole system up to time T and we have used the fact that $\sum_\alpha N_\alpha^{(h)}(T) = 2N^{(tp)}(T)$. Also in the limit of large T, we have in the leading order of T,

$$\langle N^{(tp)}(T)\rangle \simeq a(\bar{\rho})TL, \tag{87}$$

where $a(\bar{\rho})$ is the activity at density $\bar{\rho}$. By summing Eq. (81) over all particles,

$$\sum_\alpha \langle X_\alpha^2(T)\rangle \simeq 2\mathcal{D}_s(\bar{\rho})TN, \tag{88}$$

and then by using Eqs. (87) and (88) in Eq. (86), we obtain the relation as given in Eq. (85). In Fig. 6 (top panel), we plot typical trajectories of a particular tagged particle for different densities $\rho = 0.97$ (violet square points), 1.5 (green circular points), 2.0 (blue triangular points) as a function of scaled time. In Fig. 6 (bottom panel), we plot the mean square fluctuation of tagged particle displacement (solid red line) up to time T, $\langle\langle X^2(T)\rangle\rangle/2T$, as a function of $\Delta = \rho - \rho_c$, where the double angular braces $\langle\langle X^2(T)\rangle\rangle = \sum_\alpha \langle X_\alpha^2(T)\rangle/N$ denote the average over trajectories as well as particles; in simulations, during the particle transfer at any site i, two particles are chosen randomly from a particular stack. Our theoretical expression of the density dependent self-diffusion coefficient $\mathcal{D}_s(\rho)$, as given in the equality Eq. (85), is also plotted (dashed black line); one can see an excellent agreement between the simulation and the theoretical prediction. For comparison, we also plot the bulk-diffusion coefficient $D(\bar{\rho})$ (dot-dashed blue line), defined in Eq. (7). Here one

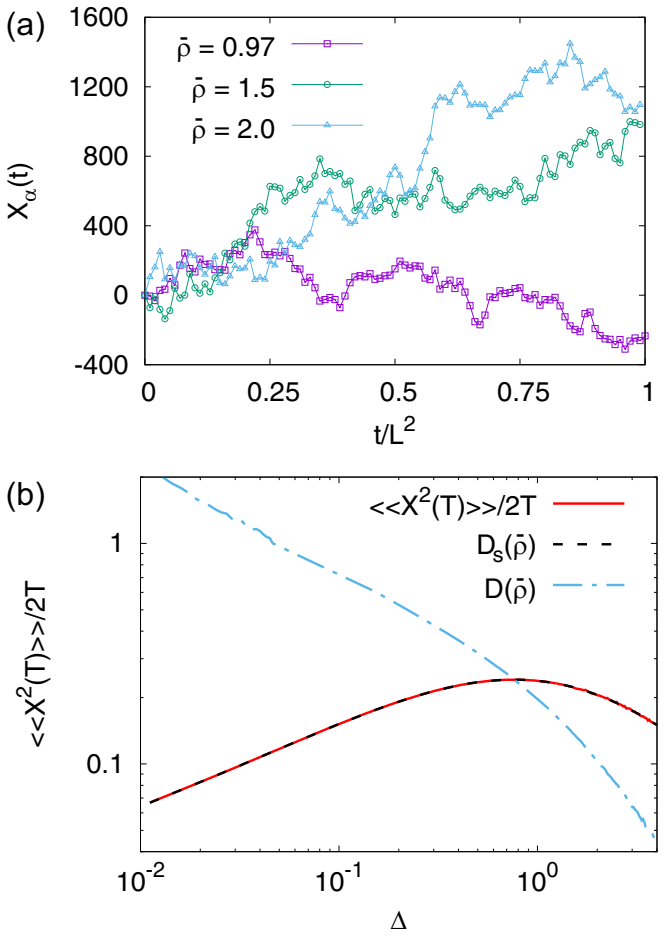

FIG. 6. In the top panel, we display the typical space-time trajectories for three tagged particles corresponding to the densities $\rho = 0.97$ (violet square points), 1.5 (green circular points), 2.0 (blue triangular points), respectively, with the scaled time axis. In the bottom panel, we plot the mean-square fluctuation of tagged particle displacement up to time T (solid red line) as a function of relative density Δ, where the double angular braces $\langle\langle X^2(T)\rangle\rangle = \sum_\alpha \langle X_\alpha^2(T)\rangle/N$ denote the average over trajectories as well as particles. Simulations (solid red line) show excellent agreement with the theoretically obtained self-diffusion coefficient $\mathcal{D}_s(\bar{\rho})$ (dashed black line) as in Eq. (85). In the same panel, we also plot the bulk-diffusion coefficient $D(\bar{\rho}) = a'(\bar{\rho})$ as a function of $\Delta = \bar{\rho} - \rho_c$ (dot-dashed blue line), using Eq. (7) from simulation, which has a contrasting behavior as compared with the self-diffusion coefficient $\mathcal{D}_s(\bar{\rho})$.

should note that the self-diffusion coefficient $\mathcal{D}_s(\bar{\rho})$ and the bulk-diffusion coefficient $D(\bar{\rho})$ are, in principle, two different quantities and strikingly they have quite contrasting behavior, especially near criticality. Indeed, upon approaching criticality where activity decays as $a(\bar{\rho}) \sim (\bar{\rho} - \rho_c)^{\beta}$ with $\beta < 1$, the self-diffusion coefficient being the ratio of activity to density [see Eq. (85)] vanishes as $\mathcal{D}_s(\bar{\rho}) \sim (\bar{\rho} - \rho_c)^{\beta}$—exactly in the same manner as the activity behaves near criticality, but the bulk-diffusion coefficient being derivative of activity with respect to the density [see Eq. (7)] diverges as $D(\bar{\rho}) \sim 1/(\bar{\rho} - \rho_c)^{1-\beta}$ [41,42]. Moreover, far from criticality and in the limit of large density $\bar{\rho} \gg 1$, although the self-diffusion coefficient and the bulk-diffusion coefficient both vanish, they do so in different manners. In that case, as the activity is expected to behave as $a(\bar{\rho}) \simeq 1 - \text{const.}/\bar{\rho}$, the self-diffusivity decays as $\mathcal{D}_s(\bar{\rho}) \sim 1/\bar{\rho}$, but the bulk-diffusivity decays much faster, $D(\bar{\rho}) \sim 1/\bar{\rho}^2$. Lastly, in the active phase, where $\bar{\rho} > \rho_c$, while the bulk-diffusion coefficient $D(\bar{\rho})$ is a monotonically decreasing function of density $\bar{\rho}$ shown in Fig. 6, the self-diffusion coefficient $\mathcal{D}_s(\bar{\rho})$ is however a nonmonotonic function of $\bar{\rho}$.

Importantly, unlike in the symmetric simple exclusion process where both the time-integrated bond current and the tagged particle displacement fluctuations grow subdiffusively as $T^{1/2}$ [52,54], in the conserved Manna sandpile only the current fluctuation grows subdiffusively, whereas the tagged particle displacement fluctuation always grows linearly with time. This is perhaps not surprising, given the fact that, in the Manna sandpile, there are no restrictions in the particle crossings, which are otherwise not allowed in the symmetric exclusion process.

F. Mass fluctuation and power spectrum

In the previous sections, we studied various properties of current fluctuations in detail. Similarly, in this section, starting from the microscopic update rules combined with the previously introduced truncation scheme, we shall derive various dynamic properties of mass fluctuations. The basic quantity is the two-point dynamic correlation function $C_r^{mm}(t,t') = \langle m_0(t) m_r(t')\rangle - \langle m_0(t)\rangle\langle m_r(t')\rangle$. By using the microscopic update rules, we write the time evolution equation for $C_r^{mm}(t,0) \equiv C_r^{mm}(t)$ as

$$\frac{d}{dt} C_r^{mm}(t) = \sum_k \Delta_{0,k} \langle \hat{a}_k(t) m_r(0)\rangle. \tag{89}$$

Using the earlier truncation approximation Eq. (23), we write the above equation as

$$\frac{d}{dt} C_r^{mm}(t) \simeq a'(\bar{\rho}) \sum_k \Delta_{r,k} C_k^{mm}(t). \tag{90}$$

The solution of Eq. (90) can be written by using the Fourier representation as

$$\tilde{C}_q^{mm}(t) \simeq e^{-a'(\bar{\rho})\lambda_q t} \tilde{C}_q^{mm}(0), \tag{91}$$

where $\tilde{C}_q^{mm}$ is the Fourier transform of C_r^{mm}. The equal-time mass correlation can be solved by using the approximation Eq. (23) in Eq. (36) and we can write the time evolution of $C_r^{mm}(t,t)$ in the steady state as

$$\frac{d}{dt} C_r^{mm}(t,t) \simeq 2a'(\bar{\rho}) \sum_k \Delta_{0,k} \langle m_k m_r\rangle + B_r = 0. \tag{92}$$

Similar to what was done earlier to solve Eq. (36), the above equation can be solved exactly using a generating function,

$$G(z) = \frac{1}{a'(\bar{\rho})}\left(\frac{3a(\bar{\rho})}{2} - \frac{a(\bar{\rho})}{4} z\right). \tag{93}$$

According to the above generating function, we have the steady-state correlations $C_0^{mm} = \langle m_0^2\rangle - \bar{\rho}^2 = 3a/2a'$, $C_1^{mm} = \langle m_0 m_1\rangle - \bar{\rho}^2 = -a/4a'$ and all other correlations being zero. Thus we immediately arrive at a relation between the scaled subsystem-mass fluctuation and the activity,

$$\sigma^2(\rho) \equiv \lim_{l\to\infty} \frac{\langle (\Delta M_l)^2\rangle}{l} = \sum_{r=-\infty}^{r=\infty} C_r^{mm} = \frac{a(\bar{\rho})}{a'(\bar{\rho})}, \tag{94}$$

where $\Delta M_l = M_l - \langle M_l\rangle$. Now, by using Eqs. (7) and (68), the above identity can be recast into a nonequilibrium version of the Green-Kubo-like relation [41],

$$\sigma^2(\bar{\rho}) = \frac{\sigma_Q^2(\bar{\rho})}{2D(\bar{\rho})}, \tag{95}$$

connecting the (scaled) subsystem-mass fluctuation $\sigma^2(\bar{\rho})$, the (scaled) subsystem-current fluctuation $\sigma_Q^2(\bar{\rho})$, and the bulk-diffusion coefficient $D(\bar{\rho})$ (a slightly different form of the above relation is usually referred as the Einstein relation in the literature [41,51]). Remarkably, the fluctuation relation in Eq. (94) implies that the scaled subsystem mass fluctuation $\sigma^2(\bar{\rho})$ varies linearly with the relative density Δ, i.e., $\sigma^2(\bar{\rho}) \sim \Delta^{1-\delta}$ with $\delta = 0$ [41]; interestingly, such behavior was indeed previously observed in simulations [59] in a variant of the conserved Manna sandpile, which is believed to be in the same universality class as that studied here.

Next we write the solution of Eq. (91) using the generating function in Eq. (93) as

$$\tilde{C}_q^{mm}(t) \simeq e^{-a'(\bar{\rho})\lambda_q t} \frac{a(\bar{\rho})}{a'(\bar{\rho})}\left(1 + \frac{\lambda_q}{4}\right). \tag{96}$$

Finally, using the inverse Fourier transformation, we get

$$C_r^{mm}(t) \simeq \frac{1}{L}\sum_q e^{-iqr} e^{-a'(\bar{\rho})\lambda_q t} \frac{a(\bar{\rho})}{a'(\bar{\rho})}\left(1 + \frac{\lambda_q}{4}\right). \tag{97}$$

We now consider subsystem mass $M_l(t) = \sum_{r=0}^{l-1} m_r(t)$ for $l < L$ and calculate the equal-time correlation function for mass $C^{M_l M_l}(t,0) \equiv C^{M_l M_l}(t)$ by using the following expression:

$$C^{M_l M_l}(t) = l C_0^{mm}(t) + \sum_{r=1}^{l-1} (l-r)\left[C_r^{mm}(t) + C_{-r}^{mm}(t)\right]. \tag{98}$$

Then by substituting Eq. (97) in Eq. (98), we get the equal-time correlation for subsystem mass,

$$C^{M_l M_l}(t) \simeq \frac{1}{L}\sum_q e^{-a'(\bar{\rho})\lambda_q t} \frac{a(\bar{\rho})}{a'(\bar{\rho})}\left(1 + \frac{\lambda_q}{4}\right)\frac{\lambda_{lq}}{\lambda_q}. \tag{99}$$

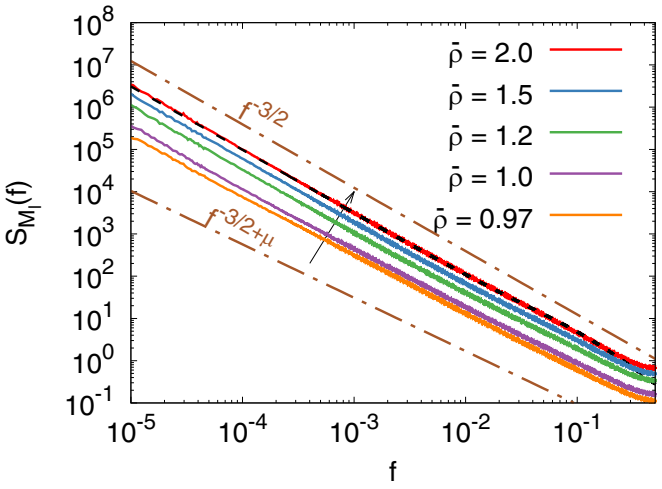

FIG. 7. Power spectrum of subsystem mass fluctuations are plotted for $L = 1000$ and $l = 500$. The solid lines represent the simulation data for the densities $\bar{\rho} = 2.0$ (red), 1.5 (blue), 1.2 (green), 1.0 (purple), 0.97 (orange), respectively. The top-most guiding line represents the $f^{-3/2}$ (away from criticality) behavior [Eq. (104)], whereas the bottom-most guiding line represents $f^{-\Psi_M}$ (near criticality) behavior [Eq. (105)] where $\Psi_M = 3/2 - \mu \approx 1.26$. The dashed black line represents the theoretical result Eq. (103) for $\rho = 2.0$. The arrow across the solid lines signifies the ascending order of densities $\bar{\rho}$.

For $t = 0$, the correlation function $C^{M_l M_l}(0)$ is nothing but the equal-time subsystem mass fluctuation, which can be written in the large system size $L \to \infty$ limit as given below:

$$C^{M_l M_l}(0) = \langle (M_l - \langle M_l \rangle)^2 \rangle = \frac{a(\bar{\rho})}{a'(\bar{\rho})} l \left[1 + \frac{1}{2l} \right]. \tag{100}$$

Then, by taking the large subsystem size $l \to \infty$ limit, where $1 \ll l \ll L$, we recover the Einstein relation, already derived in Eq. (94). Moreover the asymptotic form of Eq. (99) can be written as

$$C^{M_l M_l}(t) - C^{M_l M_l}(0) \simeq -\frac{2a(\bar{\rho})}{\sqrt{\pi a'(\bar{\rho})}} t^{\frac{1}{2}} \tag{101}$$

for large time $1 \ll t \ll L^2$; see Appendix B 4 for details. Using the Fourier transform of Eq. (99), we write the power spectrum of the subsystem mass fluctuation as

$$S_M(f) = \lim_{T \to \infty} \int_{-T}^{T} dt C^{M_l M_l}(t) e^{2\pi i f t}, \tag{102}$$

which can be written by using Eq. (99) as

$$S_M(f) = \frac{1}{L} \sum_q \frac{a(\bar{\rho})}{a'(\bar{\rho})} \left(1 + \frac{\lambda_q}{4} \right) \frac{2\lambda_q a'(\bar{\rho})}{\lambda_q^2 a'(\bar{\rho})^2 + 4\pi^2 f^2} \frac{\lambda_{lq}}{\lambda_q}. \tag{103}$$

In Fig. 7, we plot the power spectrum of the subsystem mass fluctuation, obtained from simulation for $L = 1000$ and $l = 500$ in solid lines, for various densities $\bar{\rho} = 2.0$ (red line), $\bar{\rho} = 1.5$ (blue line), $\bar{\rho} = 1.2$ (green line), $\bar{\rho} = 1.0$ (purple line), $\bar{\rho} = 0.97$ (orange line), where the arrow across the solid lines denotes the ascending order of the density $\bar{\rho}$. We compare the analytical expression (103) (dotted black line) with the simulation result for $\bar{\rho} = 2.0$ (solid red line), which is in excellent agreement with theory. The asymptotic expression of the power spectrum in Eq. (103) can be obtained by simplifying the integral as given below:

$$S_M(f) = 4a(\bar{\rho}) \int_{1/L}^{1/2} dx \frac{\lambda(lx)[1 + \lambda(x)/4]}{\lambda^2(x) a'^2(\bar{\rho}) + 4\pi^2 f^2}$$
$$\simeq \frac{a(\bar{\rho})}{2\sqrt{\pi^3 a'(\bar{\rho})}} f^{-\frac{3}{2}}. \tag{104}$$

Here, in the first step, we have replaced the sum in the right-hand side of Eq. (103) as an integral $(1/L)\sum_q \to \int_0^{2\pi} dq$ in the limit $L \to \infty$ and we used $q = 2\pi x$, $\lambda(x) = 4\pi^2 x^2$, and Eq. (75); see Appendix B 5 for details. The above asymptotic form of the power spectrum can be used to calculate the behavior near criticality by using the dimensional scaling argument as performed before in Eq. (47) where we write $a/(a')^{1/2} \sim f^{\mu}$. In other words, near criticality, the decay of the power spectrum $S_M(f)$ as a function of frequency f becomes slower and is given by

$$S_M(f) \sim f^{-\psi_M}, \tag{105}$$

where $\psi_M = 3/2 - \mu$. In Fig. 7, we plot $S_M(f)$ as a function of frequency for densities $\bar{\rho} = 2.0$ (red), 1.5 (orange), 1.2 (blue), 1.0 (green), 0.97 (violet); we observe that, as one approaches criticality, the decay of the power spectrum indeed becomes slightly slower, in accordance with our theoretical prediction in Eq. (105). The slower decay of the power spectrum up on approaching criticality can be physically understood from the current power spectrum as follows. Due to the slower temporal growth of the time-integrated bond current fluctuation [see Eq. (47)], the near-critical subsystem mass correlation also decays slower as a function of time, i.e.,

$$C^{M_l M_l}(t) - C^{M_l M_l}(0) \sim -t^{1/2-\mu}, \tag{106}$$

which is due to the fact that the time-integrated current grows slower with time and consequently the subsystem tends to retain a particular amount of mass for a much longer period. Indeed, this phenomenon can be thought of as the hyperuniformity of mass fluctuations in the temporal domain—a dynamic hyperuniformity of mass fluctuation, analogous to that of current fluctuations as described previously in Eq. (47).

We note that the two exponents $\psi_{\mathcal{J}}$ and ψ_M for the current and mass power spectra defined in Eqs. (77) and (105), respectively, are in fact related, due to the mass conservation as expressed in the continuity equation (8). By using the Fourier transform of an observable $A_r(t) = \int_{-\infty}^{\infty} df \sum_q e^{-2\pi i f t} e^{-iqr} \tilde{\mathcal{A}}_q(f)$ we can write Eq. (8) as $-2\pi i f \tilde{\mathcal{M}}_q(f) = \tilde{\mathcal{J}}_q(f)(e^{iq} - 1)$. On a large scale $q \to 0$, we have

$$S_M(f) \sim f^{-2} S_{\mathcal{J}}(f), \tag{107}$$

and therefore, from Eqs. (77) and (105), we obtain the scaling relation

$$\psi_{\mathcal{J}} = 2 - \psi_M. \tag{108}$$

III. SUMMARY AND CONCLUSIONS

In this paper, we study the steady-state dynamical properties of current and mass in the active phase of the one-dimensional conserved Manna sandpile, and we establish a direct quantitative relationship between the system's static and dynamic properties. First starting with a microscopic dynamical description, we introduce a truncation scheme, that is approximate and is expected to be valid only for long (hydrodynamic) times but allows us to theoretically investigate the time-dependent (two-point, unequal-time) correlation functions for current and mass, as well as the associated power spectra. In particular, we find that, in the thermodynamic limit, the two-point time-dependent correlation function for the (bond) current has a delta peak at time $t = 0$ and, for time $t > 0$, the correlation is *negative* and a long-ranged one, decaying as $t^{-(3/2+\mu)}$. Far from criticality, we show that the exponent $\mu = 0$, resulting in a subdiffusive $T^{1/2}$ growth of the variance of the cumulative (*time-integrated*) current up to time T. This type of subdiffusive growth of temporal fluctuation, which has previously been obtained in symmetric simple exclusion processes [52], is somewhat expected for diffusive systems with normal fluctuation properties, such as sandpiles away from criticality [42]. However, the scenario changes near the critical point. Indeed, as one approaches criticality, the activity in the system vanishes, contributing to an anomalous suppression of the temporal current fluctuations and thus a positive value of the exponent $\mu > 0$, which has been expressed in terms of the standard static exponents [see Eq. (48)]; likewise, near criticality, the power spectrum of current at low frequency f varies as $f^{1/2+\mu}$. A similar argument can be made for the temporal subsystem-mass fluctuation, which is induced by the boundary currents and is also suppressed near criticality because the current fluctuation is suppressed. The anomalously reduced mass fluctuation is manifested in the corresponding power spectrum, which, at low frequency and near criticality, varies as $f^{-3/2+\mu}$ with $\mu > 0$; on the other hand, far from criticality, the exponent $\mu = 0$, implying an $f^{-3/2}$ power spectrum, expected in a normal diffusive system. We also derive, within our theory, a nonequilibrium version of the Green-Kubo-like fluctuation-response relation [see Eq. (95)], or the Einstein relation [41,51], which connects dynamic and static fluctuations in the system. Indeed our theoretical analysis suggests that, with appropriate (diffusive) rescaling of space and time, the fluctuation properties of the Manna sandpile should be governed by a continuum fluctuating hydrodynamic description as formulated in the recently developed macroscopic fluctuation theory for diffusive systems [41,51].

We finally investigate the mean-square displacement of tagged particles and show that the self-diffusion coefficient for an individual tagged particle is identically equal to the ratio of the activity to density [see first equality in Eq. (85)]. The identity readily explains a previous simulation observation of Ref. [27] that the self-diffusion coefficient in the Manna sandpile vanishes in precisely the same fashion as the activity does upon approaching criticality. Notably, the near-critical behavior of the self-diffusion coefficient differs markedly from that of the bulk-diffusion coefficient, which was previously identified in Refs. [41,42] as the derivative $a'(\bar{\rho})$ of the activity with respect to density $\bar{\rho}$ and clearly diverges near criticality. Furthermore, while the bulk-diffusion coefficient is a monotonic function of density, the self-diffusion coefficient is a nonmonotonic one. Interestingly, the self-diffusion coefficient can be related to the current fluctuation in the system as expressed in the second equality in Eq. (85).

Our findings are reminiscent of somewhat similar observations of *dynamic hyperuniformity*, where the existence of anticorrelations in the temporal fluctuations in sandpiles were pointed out [46,60]. However, until recently [41], the precise relationship between dynamic and static fluctuations, such as that between mass and current fluctuations, was unknown, and is encoded in the Green-Kubo-like fluctuation relation as derived here in Eq. (95). The relationship demonstrates that there are indeed two mechanisms responsible for the vanishing of mass fluctuation near criticality: Physically, the anomalously suppressed current fluctuation, combined with the diverging bulk-diffusion coefficient, near criticality result in the vanishing, or hyperuniform, density fluctuation observed recently in the conserved Manna sandpiles [33].

Our results are in fact a consequence of mass conservation as reflected in the scaling relation (108) and are thus expected to be applicable in a broad class of conserved sandpiles. As our analysis suggests, the anomalous suppression of current fluctuations near criticality could be a generic feature of the *hyperuniform* state of matter and should serve as the *dynamical* signature of such states, which have been observed in similar other systems in the recent past [59,61]. In particular, our findings could help in determining the precise dynamical nature of the off- and near-critical states in sandpiles by shedding light on the microscopic dynamical origin of long-ranged temporal correlations in these systems.

ACKNOWLEDGMENTS

We thank Deepak Dhar for useful discussions and comments on the paper. A.M. acknowledges financial support from the Department of Science and Technology, India [Fellowship No. DST/INSPIRE Fellowship/2017/IF170275] for part of the work carried out under his senior research fellowship. We acknowledge the Thematic Unit of Excellence on Computational Materials Science, funded by the Department of Science and Technology, India for the computational facility. P.P. acknowledges the Science and Engineering Research Board (SERB), India, under Grant No. MTR/2019/000386, for financial support.

APPENDIX A: SOME ALGEBRAIC IDENTITIES AND SPECIAL INTEGRALS

We can deduce several algebraic properties of λ_n, which are the following:

$$\sum_{n=1}^{L-1} \frac{\lambda_{nl}}{\lambda_n^2} = \frac{1}{12} l(l-L)(l^2 - lL - 2), \tag{A1}$$

$$\sum_{n=1}^{L-1} \frac{1}{\lambda_n} = \frac{L^2 - 1}{12}, \tag{A2}$$

$$\sum_{n=1}^{L-1} \frac{\lambda_{nr}}{\lambda_n} = r(L-r), \tag{A3}$$

$$\sum_{r=1}^{l-1} 2(l-r)(2-\lambda_{rn}) = 2\left(\frac{\lambda_{ln} - l\lambda_n}{\lambda_n}\right), \tag{A4}$$

$$\sum_{n=1}^{L-1} \lambda_{nl} = 2L, \text{ for } l = 1, 2, \ldots. \tag{A5}$$

Equation (A2) is a special case of Eq. (A1) for $l = 1$.

The integrals that appear in the context of asymptotic analysis, i.e., in Eq. (76) and later in Eq. (B23), have very generic solutions in terms of hypergeometric functions. Generically, we can write these integrals in the following form:

$$I(y) = \int_0^y dz \frac{z^{-k}}{1+z} = \frac{y^{1-k}\, {}_2F_1(1, 1-k; 2-k; -y)}{1-k}, \tag{A6}$$

where ${}_2F_1$ is the hypergeometric function [62], defined as

$${}_2F_1(a, b; c; z) = \frac{\Gamma(c)}{\Gamma(b)\Gamma(c-b)} \times \int_0^1 dt t^{b-1}(1-t)^{c-b-1}(1-tz)^{-a}. \tag{A7}$$

In the limit of $y \to \infty$, we have

$$\lim_{y\to\infty} I(y) = \sqrt{2}\pi \text{ for } k = \tfrac{1}{4}, \tfrac{3}{4}. \tag{A8}$$

We have used the above result in Eqs. (76) and (B23) to obtain the asymptotic of the power spectrum of current and subsystem mass, respectively.

APPENDIX B: ASYMPTOTIC ANALYSIS

In this section, we provide the calculation details of the results of Eqs. (46), (52), (54), (67), and (101) presented in the main text.

1. Time-integrated bond current fluctuation

We now derive the asymptotic approximation of the time-integrated bond current correlation using Eq. (46). We can write the unequal-time time-integrated bond current correlation as

$$C_0^{\mathcal{Q}\mathcal{Q}}(t, t') = \frac{2a(\bar{\rho})}{L} t' + 2a(\bar{\rho})a'(\bar{\rho}) \frac{1}{L} \sum_q \frac{1 - e^{-\lambda_q a'(\bar{\rho})t'}}{\lambda_q^2 a'^2} \lambda_q \left(1 + \frac{\lambda_q}{4}\right) - a(\bar{\rho})a'(\bar{\rho}) \frac{1}{L} \sum_q \frac{1 - e^{-\lambda_q a'(\bar{\rho})t'} + e^{-\lambda_q a'(\bar{\rho})t} - e^{-\lambda_q a'(\bar{\rho})(t-t')}}{\lambda_q^2 a'^2} \lambda_q \left(1 + \frac{\lambda_q}{4}\right). \tag{B1}$$

In the infinite system size limit $L \to \infty$, we write the above sum in the following integral form:

$$C_0^{\mathcal{Q}\mathcal{Q}}(t, t') \simeq 4a'(\bar{\rho})a(\bar{\rho}) \int_0^{1/2} dx \frac{1 - e^{-\lambda(x)a'(\bar{\rho})t'}}{\lambda(x)^2 a'(\bar{\rho})^2} \lambda(x) \left(1 + \frac{\lambda(x)}{4}\right) - 2a'(\bar{\rho})a(\bar{\rho}) \int_0^{1/2} dx \frac{1 - e^{-\lambda(x)a'(\bar{\rho})t'} + e^{-\lambda(x)a'(\bar{\rho})t} - e^{-\lambda(x)a'(\bar{\rho})(t-t')}}{\lambda^2(x) a'^2(\bar{\rho})} \lambda(x) \left(1 + \frac{\lambda(x)}{4}\right). \tag{B2}$$

Note that the integral in the above equation can be expressed in terms of an integral of the form as given below:

$$a(\bar{\rho})a'(\bar{\rho}) \int_0^{1/2} dx \frac{1 - e^{-\lambda(x)a'(\bar{\rho})t'}}{\lambda^2(x) a'^2(\bar{\rho})} \lambda(x) \left(1 + \frac{\lambda(x)}{4}\right) \simeq \frac{a(\bar{\rho})\sqrt{t'}}{2\sqrt{\pi a'(\bar{\rho})}}, \tag{B3}$$

where, for $t \gg 1$, we have defined $x = [y/4\pi^2 a'(\bar{\rho})t']^{1/2}$ and used $\lambda(x) \simeq 4\pi^2 x^2$ and $\int_0^\infty dy y^{-3/2}(1 - e^{-y}) = 2\sqrt{\pi}$ to explicitly calculate the integral. Using Eq. (B3) in each of the relevant terms of the right-hand side in Eq. (B2) and then after some straightforward algebraic manipulations, we obtain the following asymptotic form of the time-dependent integrated bond-current correlation:

$$C_0^{\mathcal{Q}\mathcal{Q}}(t, t') \simeq \frac{a(\bar{\rho})}{\sqrt{\pi a'(\bar{\rho})}} (\sqrt{t} + \sqrt{t'} - \sqrt{|t - t'|}). \tag{B4}$$

Now, by putting $t' = t \equiv T$, the above asymptotic leads to the first part (i.e., corresponding to the limit $1 \ll T \ll L^2$) of Eq. (46) in the main text.

2. Time-dependent instantaneous current correlation

The steady-state unequal-time correlation of instantaneous bond current $C_0^{\mathcal{J}\mathcal{J}}(t, 0) = \langle \mathcal{J}_0(0)\mathcal{J}_r(t)\rangle - \langle \mathcal{J}_0(0)\rangle\langle \mathcal{J}_r(0)\rangle$, for $t \geqslant 0$, is given by the following expression as derived in main text [see Eq. (51)]:

$$C_0^{\mathcal{J}\mathcal{J}}(t, 0) = \delta(t) 3a(\bar{\rho}) - a'(\bar{\rho})a(\bar{\rho}) \frac{1}{L} \sum_q e^{-a'(\bar{\rho})\lambda_q t} \lambda_q \left(1 + \frac{\lambda_q}{4}\right). \tag{B5}$$

First, we perform the time integral in a finite time domain $[-T, T]$ as given below,

$$\int_{-T}^{T} C_0^{\mathcal{J}\mathcal{J}}(t,0)dt = \Gamma_0(\bar{\rho}) - \frac{2a(\bar{\rho})}{L}\sum_q \left(1+\frac{\lambda_q}{4}\right) + 2a(\bar{\rho})\left[\frac{1}{L}\sum_q e^{-\lambda_q a'(\bar{\rho})T}\left(1+\frac{\lambda_q}{4}\right)\right], \tag{B6}$$

which, using the relations Eq. (A5) and $\Gamma_0(\bar{\rho}) = 3a(\bar{\rho})$ as in the main text in Eq. (60), we simplify the above sum as

$$\int_{-T}^{T} C_0^{\mathcal{J}\mathcal{J}}(t,0)dt = \frac{2a(\bar{\rho})}{L} + 2a(\bar{\rho})\left[\frac{1}{L}\sum_q e^{-\lambda_q a'(\bar{\rho})T}\left(1+\frac{\lambda_q}{4}\right)\right]. \tag{B7}$$

Now, first taking the infinite-system size limit, i.e., the limit $L \to \infty$, we can further write the sum as an integral,

$$\lim_{L\to\infty}\int_{-T}^{T} C_0^{\mathcal{J}\mathcal{J}}(t,0)dt = 4a(\bar{\rho})\int_0^{1/2} dx e^{-\lambda(x)a'(\bar{\rho})T}\left(1+\frac{\lambda(x)}{4}\right), \tag{B8}$$

where $q = 2\pi x$. Now using $\lambda(x) \simeq 4\pi^2x^2$, $\int_0^\infty dy e^{-y}y^{-1/2} = \sqrt{\pi}$, and a variable transformation $x = y^{1/2}/2\pi[a'(\bar{\rho})T]^{1/2}$, we can explicitly calculate the integral as in Eq. (B8) as

$$\lim_{L\to\infty}\int_{-T}^{T} C_0^{\mathcal{J}\mathcal{J}}(t,0)dt \simeq \frac{a(\bar{\rho})}{\pi\sqrt{a'(\bar{\rho})T}}\int_0^\infty dy e^{-y}y^{-1/2} = \frac{a(\bar{\rho})}{\sqrt{\pi a'(\bar{\rho})}}T^{-1/2}, \tag{B9}$$

which is the result in the main text in Eq. (52). Finally, by taking the limit $T \to \infty$, we get

$$\int_{-\infty}^{\infty} C_0^{\mathcal{J}\mathcal{J}}(t,0)dt = 0, \tag{B10}$$

which is the result presented in main text in Eq. (53).

Similarly, we can find the asymptotic form of $c_0^{\mathcal{J}\mathcal{J}}(t,0)$ presented in main text in Eq. (54). In the limit $L \to \infty$, the temporal current correlation $c_0^{\mathcal{J}\mathcal{J}}(t,0)$ for $t > 0$ can be written as an integral, as given below:

$$c_0^{\mathcal{J}\mathcal{J}}(t,0) \simeq -2a'(\bar{\rho})a(\bar{\rho})\int_0^{1/2} dx e^{-a'(\bar{\rho})\lambda(x)t}\lambda(x)\left(1+\frac{\lambda(x)}{4}\right). \tag{B11}$$

Now, again using $\lambda(x) \simeq 4\pi^2x^2$ and a variable transformation $x = y^{1/2}/2\pi[a'(\bar{\rho})T]^{1/2}$, we calculate the above integral as

$$c_0^{\mathcal{J}\mathcal{J}}(t,0) \simeq -\frac{a(\bar{\rho})}{\sqrt{4\pi^2a'(\bar{\rho})}}t^{-3/2}\int_0^\infty dy\sqrt{y}e^{-y}, \tag{B12}$$

where we have ignored the subleading term $O(t^{-5/2})$. Finally, using $\int_0^\infty dy\sqrt{y}e^{-y} = \sqrt{\pi}/2$, we get the result presented in main text in Eq. (54),

$$c_0^{\mathcal{J}\mathcal{J}}(t,0) \simeq -\frac{a(\bar{\rho})}{4\sqrt{\pi a'(\bar{\rho})}}t^{-3/2}. \tag{B13}$$

3. Spacetime-integrated current fluctuation

Here we derive the asymptotic dependence of Eq. (66) on subsystem size l and time T [see Eq. (67)]; first by taking the limit $T \gg 1$ and $l \gg 1$ and then followed by the reverse order of limit $l \gg 1$ and $T \gg 1$. In both cases, we take infinite system size limit $L \to \infty$, therefore $l/L \to 0$ is always satisfy.

a. Case I: $T \gg 1$, $l \gg 1$

In this case, we write Eq. (66) in the following simplified form:

$$\langle \bar{Q}^2(l,T)\rangle = \frac{2a(\bar{\rho})Tl^2}{L} + 2a(\bar{\rho})a'(\bar{\rho})\frac{1}{L}\sum_q \frac{1-e^{-a'(\bar{\rho})\lambda_q T}}{\lambda_q^2 a'^2}\left(1+\frac{\lambda_q}{4}\right)\lambda_{ql}. \tag{B14}$$

In the limit $L \to \infty$, the sum in the above equation can be converted in to the following integral:

$$\langle \bar{Q}^2(l,T)\rangle \simeq 4a(\bar{\rho})a'(\bar{\rho})\int_0^{1/2} dx \frac{1-e^{-a'(\bar{\rho})\lambda(x)T}}{\lambda^2(x)a'^2}\left(1+\frac{\lambda(x)}{4}\right)\lambda(lx). \tag{B15}$$

Using the approximation $\lambda(lx) \simeq 4\pi^2l^2x^2$ for finite subsystem size l and a variable transformation $x = y^{1/2}/2\pi[a'(\bar{\rho})T]^{1/2}$, we get

$$\frac{1}{lT}\langle \bar{Q}^2(l,T)\rangle \simeq \frac{a(\bar{\rho})}{\pi\sqrt{a'(\bar{\rho})}}\frac{l}{\sqrt{T}}\int_0^\infty dy(1-e^{-y})y^{-3/2} = \frac{2a(\bar{\rho})}{\sqrt{\pi a'(\bar{\rho})}}\frac{l}{\sqrt{T}}, \tag{B16}$$

where we use $\int_0^\infty dy(1-e^{-y})y^{-3/2} = 2\sqrt{\pi}$. This result appears in Eq. (67) of the main text.

b. Case II: $l \gg 1$, $T \gg 1$

To compute the asymptotic form in this limit, we use the approximation $\lambda(lx) \simeq 2$ to write Eq. (66) in the following form:

$$\frac{1}{lT}\langle \bar{Q}^2(l,T)\rangle_c \simeq 2a(\bar{\rho}) + \frac{a(\bar{\rho})}{l} - \frac{8a(\bar{\rho})a'(\bar{\rho})}{lT}\int_0^{1/2} \frac{a'(\bar{\rho})\lambda(x)T - 1 + \exp\left[-\lambda(x)a'(\bar{\rho})T\right]}{\lambda^2(x)a'^2(\bar{\rho})}\left(1+\frac{\lambda(x)}{4}\right). \tag{B17}$$

Again using the variable transform $x = y^{1/2}/2\pi[a'(\bar{\rho})T]^{1/2}$ and $\int_0^\infty dy(y-1+e^{-y})y^{-5/2} = 4\sqrt{\pi}/3$, we get

$$\begin{aligned}\frac{1}{lT}\langle \bar{Q}^2(l,T)\rangle_c &\simeq 2a(\bar{\rho}) + \frac{a(\bar{\rho})}{l} - \frac{2a(\bar{\rho})a'(\bar{\rho})}{lT}\int_0^\infty dy(y-1+e^{-y})y^{-5/2}\frac{T^{3/2}}{\pi\sqrt{a'(\bar{\rho})}} \\ &= 2a(\bar{\rho}) + \frac{a(\bar{\rho})}{l} - \frac{8a(\bar{\rho})}{3}\sqrt{\frac{a'(\bar{\rho})}{\pi}}\frac{\sqrt{T}}{l},\end{aligned} \tag{B18}$$

which also appears in Eq. (67).

4. Temporal correlation of subsystem mass

The asymptotic form of subsystem mass temporal correlation $C^{M_lM_l}(t,0)$ that appears in Eq. (101) is derived here. At $t=0$, $C^{M_lM_l}(t,0)$ is a maximum and, after that, it decays as a function of time t. So, in order to extract the temporal dependence of $C^{M_lM_l}(t,0)$, we write Eq. (99) as

$$C^{M_lM_l}(0,0) - C^{M_lM_l}(t,0) = \frac{1}{L}\sum_q (1-e^{-\lambda_q a'(\bar{\rho})t})\left(1+\frac{\lambda_q}{4}\right)\frac{\lambda_{lq}}{\lambda_q}, \tag{B19}$$

which, in the limit $L\to\infty$, $l \gg 1$, can be written as

$$C^{M_lM_l}(0,0) - C^{M_lM_l}(t,0) \simeq 4\int_0^{1/2} dx \frac{a(\bar{\rho})}{a'(\bar{\rho})}(1-e^{-\lambda(x)a't})\left(1+\frac{\lambda(x)}{4}\right)\frac{1}{\lambda(x)}. \tag{B20}$$

The above equation can be further simplified using the approximation and exact results of the previous section B 3 a and we get

$$C^{M_lM_l}(0,0) - C^{M_lM_l}(t,0) = \frac{a(\bar{\rho})}{\sqrt{a'(\bar{\rho})}\pi^2}t^{\frac{1}{2}}\int_0^\infty dy y^{-\frac{3}{2}}(1-e^{-y}) = \frac{2a(\bar{\rho})}{\sqrt{\pi a'(\bar{\rho})}}t^{\frac{1}{2}}. \tag{B21}$$

Thus, we derived Eq. (101) of the main text.

5. Power spectrum of subsystem mass fluctuation

To find the asymptotic form of the power spectrum of subsystem mass fluctuation $S_{M_l}(f)$, in the limit $L\to\infty$ and $l \gg 1$, we write Eq. (103) as

$$S_{M_l}(f) \simeq \frac{8a(\bar{\rho})}{a'(\bar{\rho})}\int_0^{1/2}\frac{\lambda(x)a'(\bar{\rho})}{\lambda^2(x)a'^2(\bar{\rho}) + 4\pi^2 f^2}\left(1+\frac{\lambda(x)}{4}\right)\frac{1}{\lambda(x)}. \tag{B22}$$

Using the variable transform defined in Eq. (75) and $\lambda(x) = 4\pi^2x^2$, the above equation can be written in the following simplified form:

$$\tilde{S}_{M_l}(f) \simeq \frac{a}{2\pi^2\sqrt{2\pi a'(\bar{\rho})}}f^{-3/2}\int_0^\infty \frac{y^{-3/4}}{1+y}dy = \frac{a}{2\sqrt{\pi^3 a'(\bar{\rho})}}f^{-3/2}, \tag{B23}$$

where we used Eq. (A8) and ignored the term of $O(f^{1/2})$. Thus we derive Eq. (103), which appears in the main text.

APPENDIX C: EVOLUTION EQUATIONS OF CORRELATION FUNCTIONS

1. Different-time current-current correlation

The stochastic update rules for the different-time and different-space product function of currents $\mathcal{Q}_i(t)\mathcal{Q}_j(t')$ can be written for $t > t'$ as

$$\mathcal{Q}_i(t+dt)\mathcal{Q}_j(t') = \begin{cases} \textit{events} & \textit{probabilities} \\ [\mathcal{Q}_i(t)+1]\mathcal{Q}_j(t') & \frac{1}{2}\hat{a}_i(t)dt \\ [\mathcal{Q}_i(t)+2]\mathcal{Q}_j(t') & \frac{1}{4}\hat{a}_i(t)dt \\ [\mathcal{Q}_i(t)-1]\mathcal{Q}_j(t') & \frac{1}{2}\hat{a}_{i+1}(t)dt \\ [\mathcal{Q}_i(t)-2]\mathcal{Q}_j(t') & \frac{1}{4}\hat{a}_{i+1}(t)dt \\ \mathcal{Q}_i(t)\mathcal{Q}_j(t') & 1-\Sigma dt, \end{cases} \tag{C1}$$

where $\Sigma = 3[\hat{a}_i(t) + \hat{a}_{i+1}(t)]/4$. Using these rules, we write the evolution equation of the two-point current-current correlation function as

$$\frac{\partial}{\partial t} C_r^{\mathcal{Q}\mathcal{Q}}(t,t') = \langle [\hat{a}_0(t) - \hat{a}_1(t)]\mathcal{Q}_r(t')\rangle = \left[C_r^{\hat{a}\mathcal{Q}}(t,t') - C_{r-1}^{\hat{a}\mathcal{Q}}(t,t')\right], \tag{C2}$$

which appears in Eq. (19) in the main text.

2. Different-time mass-current correlation

The stochastic update rules for the different-time and different-space product function of mass and current $m_i(t)\mathcal{Q}_j(t')$ can be written for $t > t'$ as

$$m_i(t+dt)\mathcal{Q}_j(t') = \begin{cases} \textit{events} & \textit{probabilities} \\ [m_i(t)+1]\mathcal{Q}_j(t') & \frac{1}{2}\hat{a}_{i+1}(t)dt \\ [m_i(t)+1]\mathcal{Q}_j(t') & \frac{1}{2}\hat{a}_{i-1}(t)dt \\ [m_i(t)+1]\mathcal{Q}_j(t') & \frac{1}{4}\hat{a}_{i+1}(t)dt \\ [m_i(t)+2]\mathcal{Q}_j(t') & \frac{1}{4}\hat{a}_{i-1}(t)dt \\ [m_i(t)-2]\mathcal{Q}_j(t') & \hat{a}_i(t)dt \\ m_i(t)\mathcal{Q}_j(t') & [1-\Sigma dt], \end{cases} \tag{C3}$$

where $\Sigma = 3[\hat{a}_i(t) + \hat{a}_{i+1}(t)]/4 + \hat{a}_i(t)$. Using these rules, we write the evolution equation of the two-point mass-current correlation function as

$$\frac{\partial}{\partial t} C_r^{m\mathcal{Q}}(t,t') = \langle [\hat{a}_{L-1}(t) - 2\hat{a}_0(t) + \hat{a}_1(t)]\mathcal{Q}_r(t')\rangle \simeq a'(\bar{\rho}) \sum_k \Delta_{r,k} C_k^{m\mathcal{Q}}(t,t'), \tag{C4}$$

which appears in Eq. (26).

3. Equal-time current-current correlation

In the Manna sandpile, during each toppling two particles can hop to each neighboring site independently and it may simultaneously create current at two neighboring bonds. In the following, we write the update equation of the two point product function of integrated current:

$$\mathcal{Q}_i(t+dt)\mathcal{Q}_j(t+dt) = \begin{cases} \textit{events} & \textit{probabilities} \\ [\mathcal{Q}_i(t)-1][\mathcal{Q}_j(t)+1] & \frac{1}{2}\hat{a}_{i+1}\delta_{i+1,j}dt \\ [\mathcal{Q}_i(t)-1][\mathcal{Q}_j(t)-1] & \frac{1}{2}\hat{a}_{i+1}\delta_{i,j}dt \\ [\mathcal{Q}_i(t)+1][\mathcal{Q}_j(t)+1] & \frac{1}{2}\hat{a}_{i}\delta_{i,j}dt \\ [\mathcal{Q}_i(t)+1][\mathcal{Q}_j(t)-1] & \frac{1}{2}\hat{a}_{i}\delta_{i-1,j}dt \\ [\mathcal{Q}_i(t)-1]\mathcal{Q}_j(t) & \frac{1}{2}\hat{a}_{i+1}(1-\delta_{i+1,j}-\delta_{i,j})dt \\ [\mathcal{Q}_i(t)+1]\mathcal{Q}_j(t) & \frac{1}{2}\hat{a}_{i}(1-\delta_{i-1,j}-\delta_{i,j})dt \\ \mathcal{Q}_i(t)[\mathcal{Q}_j(t)-1] & \frac{1}{2}\hat{a}_{j+1}(1-\delta_{i-1,j}-\delta_{i,j})dt \\ \mathcal{Q}_i(t)[\mathcal{Q}_j(t)+1] & \frac{1}{2}\hat{a}_{j}(1-\delta_{i+1,j}-\delta_{i,j})dt \\ [\mathcal{Q}_i(t)+2][\mathcal{Q}_j(t)+2] & \frac{1}{4}\hat{a}_{i}\delta_{i,j}dt \\ [\mathcal{Q}_i(t)-2][\mathcal{Q}_j(t)-2] & \frac{1}{4}\hat{a}_{i+1}\delta_{i,j}dt \\ [\mathcal{Q}_i(t)+2]\mathcal{Q}_j(t) & \frac{1}{4}\hat{a}_{i}(1-\delta_{i,j})dt \\ \mathcal{Q}_i(t)[\mathcal{Q}_j(t)+2] & \frac{1}{4}\hat{a}_{j}(1-\delta_{i,j})dt \\ [\mathcal{Q}_i(t)-2]\mathcal{Q}_j(t) & \frac{1}{4}\hat{a}_{i+1}(1-\delta_{i,j})dt \\ \mathcal{Q}_i(t)[\mathcal{Q}_j(t)-2] & \frac{1}{4}\hat{a}_{j+1}(1-\delta_{i,j})dt \\ \mathcal{Q}_i(t)\mathcal{Q}_j(t) & (1-\Sigma dt), \end{cases} \tag{C5}$$

where Σdt is the probability of all events happening, as mentioned in the update rules in the time interval t and $t+dt$. Using these update rules and Eq. (23), we can write the evolution equation of the equal-time correlation function of current as

$$\begin{aligned}\frac{d}{dt}C_r^{\mathcal{Q}\mathcal{Q}}(t,t) &= \Gamma_r(t) + \langle[\hat{a}_0(t)-\hat{a}_1(t)]\mathcal{Q}_r(t)\rangle_c + \langle\mathcal{Q}_0[\hat{a}_r-\hat{a}_{r+1}]\rangle_c \\ &\simeq \Gamma_r(t) + a'\big[c_r^{m\mathcal{Q}}(t,t) - c_{r-1}^{m\mathcal{Q}}(t,t)\big] + a'\big[c_{L-r}^{m\mathcal{Q}}(t,t) - c_{L-r-1}^{m\mathcal{Q}}(t,t)\big],\end{aligned} \tag{C6}$$

where

$$\Gamma_r \equiv \Gamma_{i,j} = \tfrac{3}{2}\delta_{i,j}\langle\hat{a}_{i+1}+\hat{a}_i\rangle - \tfrac{1}{2}\delta_{i+1,j}\langle\hat{a}_{i+1}\rangle - \tfrac{1}{2}\delta_{i-1,j}\langle\hat{a}_i\rangle. \tag{C7}$$

The solution of Eq. (C6) appears in Eq. (43) in the main text.

4. Mass and integrated current correlation

The update rules of the temporal evolution equation of the product function of mass and integrated current are given as

$$m_i(t+dt)\mathcal{Q}_j(t+dt) = \begin{cases} \textit{events} & \textit{probabilities} \\ [m_i(t)+1][\mathcal{Q}_j(t)-1] & \frac{1}{2}\hat{a}_{i+1}\delta_{i,j}dt \\ [m_i(t)+1][\mathcal{Q}_j(t)+1] & \frac{1}{2}\hat{a}_{i+1}\delta_{i+1,j}dt \\ [m_i(t)-2][\mathcal{Q}_j(t)-1] & \frac{1}{2}\hat{a}_i\delta_{i-1,j}dt \\ [m_i(t)-2][\mathcal{Q}_j(t)+1] & \frac{1}{2}\hat{a}_i\delta_{i,j}dt \\ [m_i(t)+1][\mathcal{Q}_j(t)-1] & \frac{1}{2}\hat{a}_{i-1}\delta_{i-2,j}dt \\ [m_i(t)+1][\mathcal{Q}_j(t)+1] & \frac{1}{2}\hat{a}_{i-1}\delta_{i-1,j}dt \\ [m_i(t)-2][\mathcal{Q}_j(t)+2] & \frac{1}{4}\hat{a}_i\delta_{i,j}dt \\ [m_i(t)+2][\mathcal{Q}_j(t)+2] & \frac{1}{4}\hat{a}_{i-1}\delta_{i-1,j}dt \\ [m_i(t)+2][\mathcal{Q}_j(t)-2] & \frac{1}{4}\hat{a}_{i+1}\delta_{i,j}dt \\ [m_i(t)-2][\mathcal{Q}_j(t)-2] & \frac{1}{4}\hat{a}_i\delta_{i-1,j}dt \\ [m_i(t)+1]\mathcal{Q}_j(t) & \frac{1}{2}\hat{a}_{i+1}(1-\delta_{i,j}-\delta_{i+1,j})dt \\ [m_i(t)+1]\mathcal{Q}_j(t) & \frac{1}{2}\hat{a}_{i-1}(1-\delta_{i-1,j}-\delta_{i-2,j})dt \\ [m_i(t)-2]\mathcal{Q}_j(t) & \frac{1}{2}\hat{a}_i(1-\delta_{i,j}-\delta_{i-1,j})dt \\ [m_i(t)+2]\mathcal{Q}_j(t) & \frac{1}{4}\hat{a}_{i+1}(1-\delta_{i,j})dt \\ [m_i(t)-2]\mathcal{Q}_j(t) & \frac{1}{4}\hat{a}_i(1-\delta_{i-1,j})dt \\ [m_i(t)-2]\mathcal{Q}_j(t) & \frac{1}{4}\hat{a}_i(1-\delta_{i,j})dt \\ [m_i(t)+2]\mathcal{Q}_j(t) & \frac{1}{4}\hat{a}_{i-1}(1-\delta_{i-1,j})dt \\ m_i(t)[\mathcal{Q}_j(t)+1] & \frac{1}{2}\hat{a}_j(1-\delta_{i,j}-\delta_{i,j-1}-\delta_{i,j+1})dt \\ m_i(t)[\mathcal{Q}_j(t)-1] & \frac{1}{2}\hat{a}_{j+1}(1-\delta_{i,j}-\delta_{i,j+1}-\delta_{i,j+2})dt \\ m_i(t)[\mathcal{Q}_j(t)+2] & \frac{1}{4}\hat{a}_j(1-\delta_{i,j}-\delta_{i,j+1})dt \\ m_i(t)[\mathcal{Q}_j(t)-2] & \frac{1}{4}\hat{a}_{j+1}(1-\delta_{i,j}-\delta_{i,j+1})dt. \end{cases} \tag{C8}$$

Clearly, nothing happens with probability $1-\Sigma dt$, where Σdt is the sum of the probabilities of all the above events. Using these rules, we write the evolution equation of the two point mass and integrated current correlation as

$$\frac{d}{dt}C_r^{m\mathcal{Q}}(t,t) = f_r(t) + \sum_k \Delta_{r,k}C_k^{\hat{a}\mathcal{Q}}(t,t), \tag{C9}$$

where $f_r(t)$, the source term of the equal-time mass-integrated current correlation, which, in the steady state, can be written as

$$f_r(t) = \big[C_r^{m\hat{a}}(t,t) - C_{r+1}^{m\hat{a}}(t,t)\big] + \frac{7a(\bar{\rho})}{2}\delta_{0,r+1} - \frac{7a(\bar{\rho})}{2}\delta_{0,r} + \frac{a(\bar{\rho})}{2}(\delta_{0,r-1}-\delta_{0,r+2}). \tag{C10}$$

The Fourier transform of Eq. (C9) is used to get Eq. (32) in the main text.

5. Mass-mass correlation function

The equal-time mass-mass correlation function is important to calculate the mass-activity correlation function and the power spectrum of the subsystem mass. The update rules are the following:

$$m_i(t+dt)m_j(t+dt) = \begin{cases} \textit{events} & \textit{probabilities} \\ [m_i(t)+1][m_j(t)+1] & \frac{1}{2}\hat{a}_{i+1}\delta_{i,j}dt \\ [m_i(t)+1][m_j(t)-2] & \frac{1}{2}\hat{a}_{i+1}\delta_{i+1,j}dt \\ [m_i(t)+1][m_j(t)+1] & \frac{1}{2}\hat{a}_{i+1}\delta_{i+2,j}dt \\ [m_i(t)-2][m_j(t)+1] & \frac{1}{2}\hat{a}_{i}\delta_{i-1,j}dt \\ [m_i(t)-2][m_j(t)-2] & \frac{1}{2}\hat{a}_{i}\delta_{i,j}dt \\ [m_i(t)-2][m_j(t)+1] & \frac{1}{2}\hat{a}_{i}\delta_{i+1,j}dt \\ [m_i(t)+1][m_j(t)+1] & \frac{1}{2}\hat{a}_{i-1}\delta_{i-2,j}dt \\ [m_i(t)+1][m_j(t)-2] & \frac{1}{2}\hat{a}_{i-1}\delta_{i-1,j}dt \\ [m_i(t)+1][m_j(t)+1] & \frac{1}{2}\hat{a}_{i-1}\delta_{i,j}dt \\ [m_i(t)+1]m_j(t) & \frac{1}{2}\hat{a}_{i+1}\big(1-\delta_{i,j}-\delta_{i+1,j}-\delta_{i+2,j}\big)dt \\ [m_i(t)-2]m_j(t) & \frac{1}{2}\hat{a}_{i}(1-\delta_{i-1,j}-\delta_{i,j}-\delta_{i+1,j})dt \\ [m_i(t)+1]m_j(t) & \frac{1}{2}\hat{a}_{i-1}(1-\delta_{i-2,j}-\delta_{i-1,j}-\delta_{i,j})dt \\ m_i(t)[m_j(t)+1] & \frac{1}{2}\hat{a}_{j+1}(1-\delta_{i,j}-\delta_{i,j+1}-\delta_{i,j+2})dt \\ m_i(t)[m_j(t)-2] & \frac{1}{2}\hat{a}_{j}(1-\delta_{i,j-1}-\delta_{i,j}-\delta_{i,j+1})dt \\ m_i(t)[m_j(t)+1] & \frac{1}{2}\hat{a}_{j-1}(1-\delta_{i,j-2}-\delta_{i,j-1}-\delta_{i,j})dt \\ [m_i(t)+2][m_j(t)+2] & \frac{1}{4}\hat{a}_{i+1}\delta_{i,j}dt \\ [m_i(t)+2][m_j(t)-2] & \frac{1}{4}\hat{a}_{i+1}\delta_{i+1,j}dt \\ [m_i(t)-2][m_j(t)+2] & \frac{1}{4}\hat{a}_{i}\delta_{i-1,j}dt \\ [m_i(t)-2][m_j(t)-2] & \frac{1}{4}\hat{a}_{i}\delta_{i,j}dt \\ [m_i(t)+2]m_j(t) & \frac{1}{4}\hat{a}_{i+1}(1-\delta_{i,j}-\delta_{i+1,j})dt \\ [m_i(t)-2]m_j(t) & \frac{1}{4}\hat{a}_{i}(1-\delta_{i-1,j}-\delta_{i,j})dt \\ m_i(t)[m_j(t)+2] & \frac{1}{4}\hat{a}_{j+1}(1-\delta_{i,j}-\delta_{i,j+1})dt \\ m_i(t)[m_j(t)-2] & \frac{1}{4}\hat{a}_{j}(1-\delta_{i,j-1}-\delta_{i,j})dt \\ [m_i(t)-2][m_j(t)-2] & \frac{1}{4}\hat{a}_{i}\delta_{i,j}dt \\ [m_i(t)-2][m_j(t)+2] & \frac{1}{4}\hat{a}_{i}\delta_{i+1,j}dt \\ [m_i(t)+2][m_j(t)-2] & \frac{1}{4}\hat{a}_{i-1}\delta_{i-1,j}dt \\ [m_i(t)+2][m_j(t)+2] & \frac{1}{4}\hat{a}_{i-1}\delta_{i,j}dt \\ [m_i(t)-2]m_j(t) & \frac{1}{4}\hat{a}_{i}(1-\delta_{i,j}-\delta_{i+1,j})dt \\ [m_i(t)+2]m_j(t) & \frac{1}{4}\hat{a}_{i-1}(1-\delta_{i-1,j}-\delta_{i,j})dt \\ m_i(t)[m_j(t)+2] & \frac{1}{4}\hat{a}_{j-1}(1-\delta_{i,j}-\delta_{i,j-1})dt \\ m_i(t)[m_j(t)-2] & \frac{1}{4}\hat{a}_{j}(1-\delta_{i,j+1}-\delta_{i,j})dt. \end{cases} \tag{C11}$$

Clearly, nothing happens with probability $1-\Sigma dt$, where Σdt is the sum of the probabilities of all the above events. From these update rules, we can write the evolution equation of $C_r^{mm}(t,t)$ as

$$\frac{d}{dt}\langle m_i(t)m_j(t)\rangle = \sum_k \langle m_i\Delta_{j,k}\hat{a}_k + \Delta_{i,k}\hat{a}_k m_j\rangle_c + B_{i,j}, \tag{C12}$$

where

$$B_{i,j} = \tfrac{1}{2}\langle 3\hat{a}_{i-1}+8\hat{a}_i+3\hat{a}_{i+1}\rangle\delta_{i,j} - \tfrac{1}{2}\langle 4\hat{a}_{i+1}+4\hat{a}_i\rangle\delta_{i+1,j} - \tfrac{1}{2}\langle 4\hat{a}_{i-1}+4\hat{a}_i\rangle\delta_{i+1,j} + \tfrac{1}{2}\langle\hat{a}_{i+1}\rangle\delta_{i+2,j} + \tfrac{1}{2}\langle\hat{a}_{i-1}\rangle\delta_{i-2,j} \tag{C13}$$

is the source of the equal-time mass correlation. In the steady state, where $\langle\hat{a}_i(t)\rangle = a(\bar{\rho})$, we can write $B_{i,j}$ as a translationally invariant form, $B_{i,j}\equiv B_r$, as

$$B_r = 7a(\bar{\rho})\delta_{0,r} - 4a(\bar{\rho})(\delta_{0,r+1}+\delta_{0,r-1}) + \frac{a(\bar{\rho})}{2}(\delta_{0,r+2}+\delta_{0,r-2}). \tag{C14}$$

Equation (C12) appears in Eq. (36) in the main text. Using the steady-state condition, we must have $d\langle m_i m_j\rangle_c/dt = 0$, which implies

$$2\big[C_{r-1}^{m\hat{a}} - 2C_r^{m\hat{a}} + C_{r+1}^{m\hat{a}}\big] + B_r = 0. \tag{C15}$$

Equation (C15) can be solved by considering the following generating function:

$$G(z) = \sum_{r=0}^{\infty} C_r^{m\hat{a}} z^r. \tag{C16}$$

We multiply both side of Eq. (C15) with z^r and sum over r to get

$$G(z) = \frac{4C_0^{m\hat{a}} - 4zC_1^{m\hat{a}} - za[(z-8)z+14]}{4(1-z)^2}, \tag{C17}$$

where we use the identities

$$\sum_{r=0}^{\infty} C_{r-1}^{m\hat{a}} z^r = C_1^{m\hat{a}} + zG(z), \quad \sum_{r=0}^{\infty} C_{r+1}^{m\hat{a}} z^r = \frac{G(z) - C_0^{m\hat{a}}}{z}. \tag{C18}$$

As we are dealing with truncated correlation functions, in the limit $z \to 1$, we must have $\lim_{z\to 1} G(z) < \infty$. Using a new variable $w \to 1 - z$, we write Eq. (C17) as

$$G(w) = \frac{1}{4w^2}\left\{a(\bar{\rho})w^3 + 5a(\bar{\rho})w^2 + \left[a(\bar{\rho}) + 4C_1^{m\hat{a}}\right]w + -7a(\bar{\rho}) + 4C_0^{m\hat{a}} - 4C_1^{m\hat{a}}\right\}. \tag{C19}$$

For the convergence of $G(w)$ in the limit $w \to 0$, we set

$$a(\bar{\rho}) + 4C_1^{m\hat{a}} = 0, \quad -7a(\bar{\rho}) + 4C_0^{m\hat{a}} - 4C_1^{m\hat{a}} = 0, \tag{C20}$$

leading to the following exact relations:

$$C_0^{m\hat{a}} = \frac{3a(\bar{\rho})}{2}, \tag{C21}$$

$$C_1^{m\hat{a}} = -\frac{a(\bar{\rho})}{4}. \tag{C22}$$

Finally, putting Eq. (C21) in Eq. (C17) we get the generating function

$$G(z) = \frac{3a(\bar{\rho})}{2} - \frac{a(\bar{\rho})}{4}z. \tag{C23}$$

[1] B. B. Mandelbrot, *The Fractal Geometry of Nature*, 3rd ed. (W. H. Freeman and Comp., 1983).
[2] F. Frontera and F. Fuligni, Astrophys. J. **232**, 590 (1979).
[3] M. J. Aschwanden *et al.*, Space Sci. Rev. **198**, 47 (2016).
[4] L. Palmieri and H. J. Jensen, Front. Phys. **8**, 257 (2020).
[5] E. Novikov, A. Novikov, D. Shannahoff-Khalsa, B. Schwartz, and J. Wright, Phys. Rev. E **56**, R2387(R) (1997).
[6] J. Hesse and T. Gross, Front. Syst. Neurosci. **8** (2014).
[7] C. Tebaldi, Front. Phys. **8**, 616408 (2021).
[8] R. F. Voss and J. Clarke, Phys. Rev. B **13**, 556 (1976).
[9] H. J. Jensen, *Self-Organized Criticality* (Cambridge University Press, 1998).
[10] P. Bak, *How Nature Works: the Science of Self-Organized Criticality* (Oxford University Press, 1997).
[11] P. Bak, C. Tang, and K. Wiesenfeld, Phys. Rev. Lett. **59**, 381 (1987).
[12] P. Bak, C. Tang, and K. Wiesenfeld, Phys. Rev. A **38**, 364 (1988).
[13] D. Dhar and R. Ramaswamy, Phys. Rev. Lett. **63**, 1659 (1989).
[14] D. Dhar, Phys. Rev. Lett. **64**, 1613 (1990).
[15] V. B. Priezzhev, D. Dhar, A. Dhar, and S. Krishnamurthy, Phys. Rev. Lett. **77**, 5079 (1996).
[16] S. Majumdar and D. Dhar, Phys. A (Amsterdam, Neth.) **185**, 129 (1992).
[17] A. Fey, L. Levine, and D. B. Wilson, Phys. Rev. Lett. **104**, 145703 (2010).
[18] M. Podder and L. T. Rolla, J. Stat. Phys. **182**, 52 (2021).
[19] A. Cipriani, R. S. Hazra, and W. M. Ruszel, Probab. Theory Relat. Fields **172**, 829 (2018).
[20] R. Dickman, A. Vespignani, and S. Zapperi, Phys. Rev. E **57**, 5095 (1998).
[21] R. Dickman, M. Alava, M. A. Muñoz, J. Peltola, A. Vespignani, and S. Zapperi, Phys. Rev. E **64**, 056104 (2001).
[22] A. Vespignani, R. Dickman, M. A. Muñoz, and S. Zapperi, Phys. Rev. E **62**, 4564 (2000).
[23] A. Vespignani, R. Dickman, M. A. Muñoz, and S. Zapperi, Phys. Rev. Lett. **81**, 5676 (1998).
[24] P. Le Doussal and K. J. Wiese, Phys. Rev. Lett. **114**, 110601 (2015).
[25] J. J. Ramasco, M. A. Muñoz, and C. A. da Silva Santos, Phys. Rev. E **69**, 045105(R) (2004).
[26] R. Dickman, Phys. Rev. E **66**, 036122 (2002).
[27] S. D. da Cunha, R. R. Vidigal, L. R. da Silva, and R. Dickman, Eur. Phys. J. B **72**, 441 (2009).
[28] D. Dhar, Phys. A (Amsterdam, Neth.) **369**, 29 (2006).
[29] R. Dickman, M. A. Muñoz, A. Vespignani, and S. Zapperi, Braz. J. Phys. **30**, 27 (2000).
[30] F. Redig, Mathematical aspects of the abelian sandpile model, *Mathematical Statistical Physics Volume 83 Lecture Notes of the Les Houches Summer School 2005*, 70th ed. (Elsevier Science, London, England, 2006).
[31] P. Pradhan, Front. Phys. **9**, 641233 (2021).

[32] A. A. Ali, Phys. Rev. E **52**, R4595(R) (1995).
[33] D. Hexner and D. Levine, Phys. Rev. Lett. **114**, 110602 (2015).
[34] D. Hexner and D. Levine, Phys. Rev. Lett. **118**, 020601 (2017).
[35] S. Torquato and F. H. Stillinger, Phys. Rev. E **68**, 041113 (2003).
[36] S. Torquato, Phys. Rev. E **94**, 022122 (2016).
[37] U. S. Nizam, G. Makey, M. Barbier, S. S. Kahraman, E. Demir, E. E. Shafigh, S. Galioglu, D. Vahabli, S. Husnugil, M. H. Guneş *et al.*, J. Phys.: Condens. Matter **33**, 304002 (2021).
[38] R. Dandekar and D. Dhar, Europhys. Lett. **104**, 26003 (2013).
[39] R. Dandekar, Europhys. Lett. **132**, 10008 (2020).
[40] S. S. Manna, J. Phys. A: Math. Gen. **24**, L363 (1991).
[41] S. Chatterjee, A. Das, and P. Pradhan, Phys. Rev. E **97**, 062142 (2018).
[42] D. Tapader, P. Pradhan, and D. Dhar, Phys. Rev. E **103**, 032122 (2021).
[43] J. Kertesz and L. B. Kiss, J. Phys. A: Math. Gen. **23**, L433 (1990).
[44] L. Laurson, M. J. Alava, and S. Zapperi, J. Stat. Mech.: Theory Exp. (2005) L11001.
[45] H. J. Jensen, K. Christensen, and H. C. Fogedby, Phys. Rev. B **40**, 7425 (1989).
[46] R. Garcia-Millan, G. Pruessner, L. Pickering, and K. Christensen, Europhys. Lett. **122**, 50003 (2018).
[47] A. C. Yadav, R. Ramaswamy, and D. Dhar, Phys. Rev. E **85**, 061114 (2012).
[48] S. Maslov, C. Tang, and Y.-C. Zhang, Phys. Rev. Lett. **83**, 2449 (1999).
[49] M. Baiesi and C. Maes, Europhys. Lett. **75**, 413 (2006).
[50] A. Giometto and H. J. Jensen, Phys. Rev. E **85**, 011128 (2012).
[51] L. Bertini, A. De Sole, D. Gabrielli, G. Jona-Lasinio, and C. Landim, Rev. Mod. Phys. **87**, 593 (2015).
[52] T. Sadhu and B. Derrida, J. Stat. Mech.: Theory Exp. (2016) 113202.
[53] T. Sadhu and D. Dhar, J. Stat. Phys. **134**, 427 (2009).
[54] A. De Masi and P. A. Ferrari, J. Stat. Phys. **107**, 677 (2002).
[55] K. Jain, Phys. Rev. E **72**, 017105 (2005).
[56] The details of the results will be presented elsewhere.
[57] U. Marconi, A. Puglisi, L. Rondoni, and A. Vulpiani, Phys. Rep. **461**, 111 (2008).
[58] D. K. C. MacDonald, *Noise and Fluctuations*, Dover Books on Physics (Dover Publications, Mineola, 2006).
[59] D. Hexner, P. M. Chaikin, and D. Levine, Proc. Natl. Acad. Sci. U. S. A. **114**, 4294 (2017).
[60] T. Hwa and M. Kardar, Phys. Rev. Lett. **62**, 1813 (1989).
[61] L. Corte, P. M. Chaikin, J. P. Gollub, and D. J. Pine, Nat. Phys. **4**, 420 (2008).
[62] G. Gasper and M. Rahman, *Basic Hypergeometric Series* (Cambridge University Press, 2004).